

SEMMELWEIS EGYETEM
DOKTORI ISKOLA

Ph.D. értekezések

2024.

CELENG CSILLA

Szív-és érrendszeri betegségek élettana és klinikuma
című program

Programvezető: Dr. Merkely Béla, egyetemi tanár

Témavezető: Dr. Maurovich-Horvat Pál, egyetemi adjunktus

Imaging of the Coronary Arteries and Aortic Root with Computed Tomography Angiography

Doctoral Thesis

Csilla Celeng

Doctoral School of Basic Medicine
Semmelweis University



Supervisor:

Pál Maurovich-Horvat, MD, Ph.D.

Official reviewers:

Albert Varga, MD, D.Sc.

Lívía Jánoskúti, MD, Ph.D.

Head of the Final Examination Committee:

Viktor Bérczi, MD, D.Sc.

Members of the Final Examination Committee:

Attila Doros, MD, Ph.D.

László Sallai, MD, Ph.D.

Budapest, 2017

Table of Contents

Abbreviations	4
1. INTRODUCTION	6
1.1 CTA for the assessment of the coronary arteries	8
1.2 Prospectively ECG-triggered image acquisition	12
1.3 Diastolic and systolic acquisition with absolute and relative delay	13
1.4 Premedication before coronary CTA	14
1.5 Anatomy of the aortic root	15
1.6 CTA for the assessment of the aortic root	17
1.7 Determinants of the aortic root geometry: genetics versus environment	19
2. OBJECTIVES	
2.1 Defining the optimal systolic phase targets by using absolute delay	20
2.2 Defining the efficacy and safety of esmolol vs. metoprolol.....	20
2.3 Defining the heritability of the aortic root by CTA and TTE.....	20
3. METHODS	
3.1. Study design and study population for optimal systolic phase	21
3.1.1 Coronary CTA data acquisition and image analysis.....	21
3.1.2 Coronary artery velocity mapping	24
3.2. Study design and population for esmolol vs. metoprolol	26
3.2.1 Drug administration protocol and heart rate monitoring	27
3.2.2 Coronary CTA scan protocol	28
3.3. Study design and population for heritability of the aortic root.....	29
3.3.1 CTA scan and drug administration protocol.....	30
3.3.2 CTA analysis of the aortic root.....	31
3.3.3 TTE imaging of the aortic root	33
3.4 Statistical analyses	34
3.4.1 Sample size calculation for the esmolol vs. metoprolol study.....	34
3.4.2 Statistical analysis for heritability estimates.....	35
4. RESULTS	
4.1 Optimal systolic phase targets by using absolute delay	37
4.2 Efficacy and safety of esmolol vs. metoprolol.....	41
4.3 Heritability estimates of aortic root dimensions by CTA and TTE	45

5. DISCUSSION	
5.1 Systolic image reconstruction by using absolute delay	52
5.2 The use of esmolol before coronary CTA	56
5.3 Impact of the imaging method on heritability of the aortic root	59
5.4 Limitations.....	61
5.5 Future Perspectives.....	63
6. CONCLUSIONS	66
7. SUMMARY	67
8. ÖSSZEFOGLALÁS	68
9. BIBLIOGRAPHY	69
10. BIBLIOGRAPHY OF THE CANDIDATE'S PUBLICATIONS	84
10.1 Publications closely related to the present thesis.....	84
10.2 Publication not related to the present thesis.....	84
ACKNOWLEDGEMENTS	87

Abbreviations

2D	2-dimensional
3D	3-dimensional
A	area
A	additive genetic effects
AHA	American Heart Association
AIC	Akaike Information Criterion
ALARA	As Low As Reasonably Achievable
AMI	acute marginal branch
Ao	ascending aorta
BIC	Bayesian Information Criterion
BMI	body mass index
bpm	beat per minute
C	circumference
C	common environmental effects
CAD	coronary artery disease
CAVI	transcatheter caval valve implantation
CI	confidence interval
cMPR	curved multiplanar reformation
CTA	computed tomography angiography
D	mean diameter
D	dominant genetic effects
D1	diagonal 1 branch
D2	diagonal 2 branch
D _L	long diameter
D _S	short diameter
DZ	dizygotic twins
E	unique environmental effects
ECG	electrocardiography
GWAS	genome-wide association studies
HR	heart rate
ICC	intraclass correlation coefficient

ICT	isovolumic contraction time
IRB	institutional review board
IV	intravenous
kV	kilovolt
LA	left atrium
LAD	left anterior descending artery
LCX	circumflex artery
LM	left main coronary artery
LV	left ventricle
LVET	left ventricular ejection time
LVOT	left ventricular outflow tract
mAs	milliamperere-second
mg	milligram
MIP	maximum intensity projections
mL/s	milliliter/second
mm Hg	millimeter of mercury
mm/s	millimeter second
MPR	multiplanar reformation
ms	millisecond
MZ	monozygotic twins
OM1	obtuse marginal 1
P	phenotype
PDA	posterior descending artery
PEP	pre-ejection period
RA-IVC	right-atrium inferior vena cava
RCA	right coronary artery
RFCA	radiofrequency catheter-ablation
SCCT	Society of Cardiovascular Computed Tomography
TAVI	transcatheter aortic valve implantation
TGFBR	transforming growth factor-beta receptor
TTE	transthoracic echocardiography
VRT	volume rendering technique reconstructions

1. INTRODUCTION

In the past years computed tomography angiography (CTA) has become a widely adopted non-invasive imaging technique for the direct visualization of coronary artery disease (CAD). High spatial resolution of current CT scanners allows for detailed anatomical and morphological evaluation of atherosclerotic plaques, while high temporal resolution enables to acquire the fast-moving coronary arteries. In addition the 3-dimensional (3D) nature of CTA provides precise visualization of complex cardiac structures thus aiding in the planning of structural heart interventions such as transcatheter aortic valve implantation (TAVI) as one of the most successful examples. Cardiac CTA however is a technically demanding procedure and motion artifacts caused by the constant movement of the heart present the chief challenge. Therefore optimized timing of the acquisition window with the least motion is utmost importance to achieve diagnostic image quality.

One option to assess motion-free images is the synchronization of the acquisition window to the phase of the cardiac cycle with minimal coronary arterial motion. Current guidelines report the use of prospectively ECG-triggered image acquisition [1] preferably in the most tranquil period of the cardiac cycle, which at low and stable heart rates (HR) is during mid-diastole (during diastasis) [2, 3] and in patients with high HR is during end-systole [4, 5].

Another method to achieve favorable image quality is the reduction of HR. In patients undergoing coronary CTA HR should be <65 beats per minute (bpm) and optimally <60 bpm to achieve excellent image quality and low effective radiation dose [6]. Metoprolol is the first-line β -blocker for HR lowering [7-9]. However, potential contraindications and side-effects (e.g. reactive airway disease, bradycardia, hypotension) might hamper its use in a subset of patients. During coronary CTA, short and effective HR control is desirable; short-lasting intravenous (IV) esmolol therefore might be a good alternative for metoprolol. Currently, esmolol is routinely administered in the intensive care unit for the treatment of acute supraventricular arrhythmias; however, administration before coronary CTA for HR reduction is an “off-label” indication.

Motion-free images are the pre-requisite to assess accurate and reproducible measurements of anatomically complex structures. Manual adjustments might be time-consuming, with the potential for increased intra-reader and inter-reader variability.

Commercially available semi- and fully automated software algorithms aim to standardize image analysis thus providing reliable measurements, which are critical for clinical and research applications. Computer aided analysis might provide more reproducible measurements, thus reduce the frequency of reader disagreements. Furthermore, automatic post-processing of image data, will likely increase efficacy in clinical practice.

1.1 CTA for the assessment of the coronary arteries

The excellent image quality provided by high-resolution CT scanners enables direct and reliable evaluation of the coronary arteries. Prior to CTA a preliminary interpretation of prospectively ECG-triggered calcium score scan is performed. This allows for the detection of calcified lesions across the coronary arteries. Based on the area-density of the lesions the software generates the Agatston-score, which is calculated by multiplying the lesion area (mm^2) by a density factor (between 1 and 4 based on the voxel with the highest density) [10].

The non-contrast examination is followed by IV administration of iodinated contrast agent, which enables to reach uniform enhancement among coronary arteries and permits direct visualization of the coronary lumen and atherosclerotic plaques. Based on the presence and quantity of calcified plaque components atherosclerotic lesions are classified into three categories: calcified, partially calcified and non-calcified plaques [11]. The Society of Cardiovascular Computed Tomography (SCCT) released a standardized diagram that is recommended for the reporting of coronary artery lesions. The diagram is based on the American Heart Association (AHA) coronary segmentation, with an addition of the ramus intermedius (segment 17) and left posterolateral branch (segment 18) (**Figure 1**) [12].

The anatomical complexity of the coronary arteries requires cardiac specific platforms, which are capable to display the 3D dataset in all conventional reconstruction formats. These include transaxial 2-dimensional (2D) image stacks, multiplanar reformations (MPR), maximum intensity projections (MIP), curved multiplanar reformations (cMPR), and volume rendering technique (VRT) reconstructions (**Figure 2**).

Artifact-free images are the most important prerequisite for the diagnostic evaluation of the coronary arteries. Continuous motion of the heart, calcifications, image noise and poor contrast enhancement might substantially degrade the quality of the exam. The desired temporal resolution for complete motion-free image is 19 millisecond (ms) [13]. Since the temporal resolution of modern CT scanners is 75-175 ms [14] motion artifacts are often present, especially in the midsegment of the RCA [15]. “Stairstep artifacts” or according to a newer terminology “misalignment artifacts” [11] occur between reconstruction of sequential heartbeats, mainly in patients with higher or irregular HR or the presence of ectopic heartbeats (**Figure 2**).

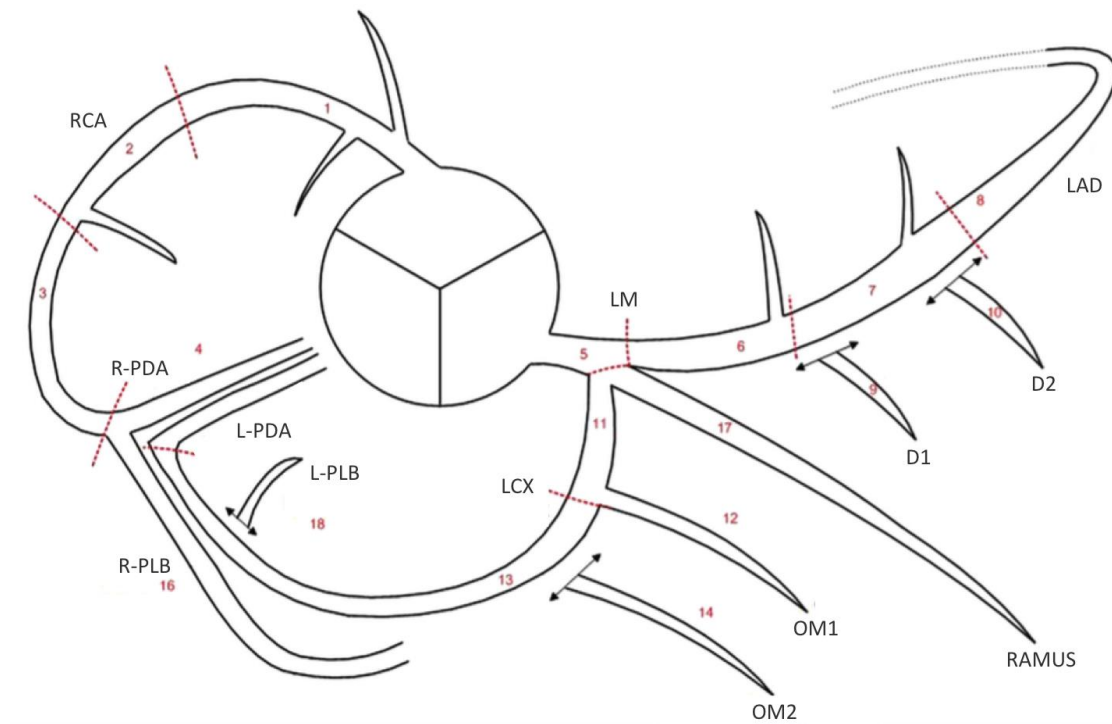


Figure 1. Coronary artery segmentation diagram by the Society of Cardiovascular Computed Tomography (SCCT) [12]

LM: left main; LAD: left anterior descending artery; D1: diagonal 1; D2: diagonal 2; LCX: circumflex artery; OM1: obtuse marginal 1; OM2: obtuse marginal 2; RCA: right coronary artery; PDA: posterior descending artery; R-PDA: PDA from RCA; L-PDA: PDA from LCX; PLB: posterolateral branch; R-PLB: PLB from RCA; L-PLB: PLB from LCX. Dashed lines represent division between RCA, LAD, and LCX and the end of the LM.

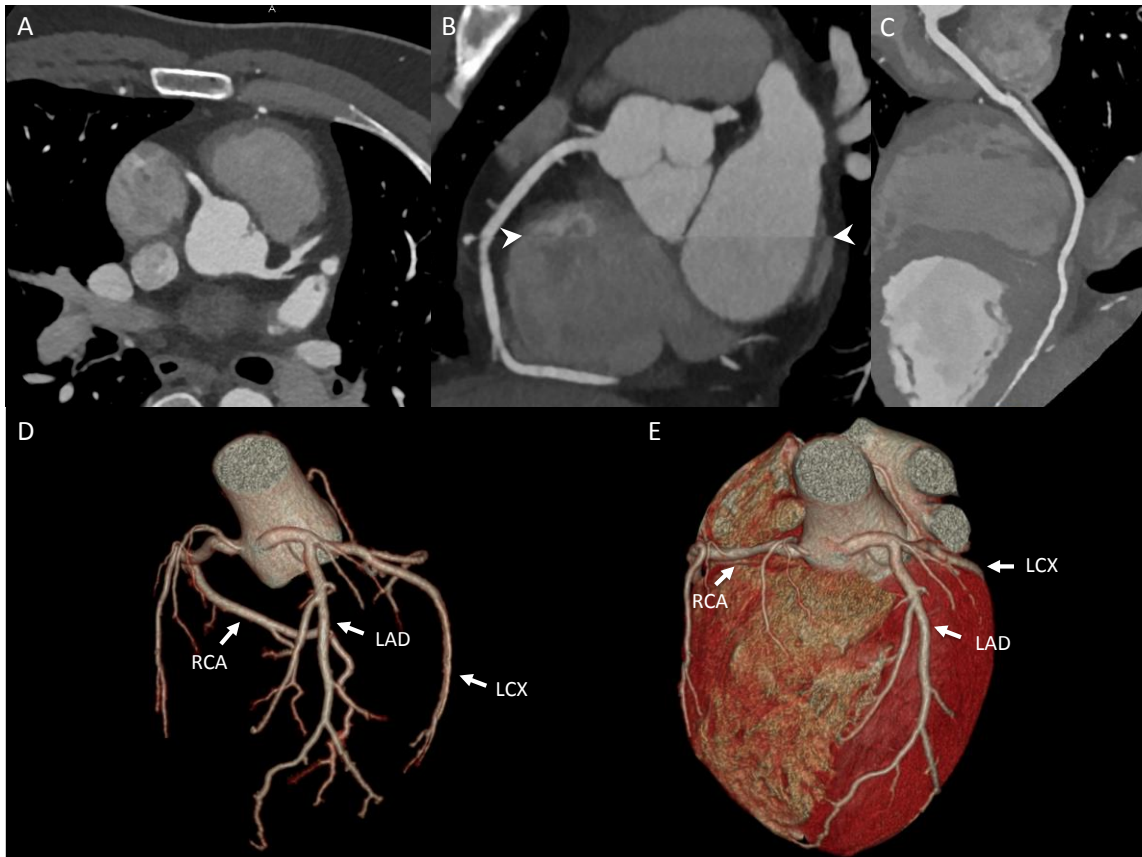


Figure 2. CTA images and volume-rendered images of the coronary arteries and the heart (*own material*)

A: axial image of the LAD and RCA; B: coronal, multiplanar, maximal intensity projection image of the RCA and misalignment artifact (white arrowheads); C: curved multiplanar image of the RCA; D: volume-rendered 3D image of the coronary tree; E: volume-rendered 3D image of the heart. LAD: left anterior descending artery; LCX: left circumflex artery; RCA: right coronary artery

One option to eliminate vessel misalignment artifacts is reconstruction of the dataset in different phases of the cardiac cycle. In general coronary arteries are optimally imaged when the heart moves the least, which occurs in mid-diastole (during diastasis). However with increasing HR this period shortens, and end-systolic reconstruction (period of the isovolumic relaxation) might render fewer motion artifacts.

Retrospective ECG gating provides continuous data acquisition during the cardiac cycle with the potential of diastolic as well as systolic image reconstruction. However concerns have been raised regarding the ALARA principle, which states that the radiation dose to a patient should be As Low As Reasonably Achievable. Currently, when performing cardiac CTA prospectively ECG-triggered scan protocol is preferred, which applies radiation only at pre-defined points of the cardiac cycle and is able to reduce the radiation exposure by 70 % [16]. Using this method however image reconstruction is limited to a pre-determined temporal-window.

Image quality can be also substantially improved by appropriate pre-medication of patients with higher heart. Previous studies demonstrated that a HR of <65 bpm yielded the least motion artifacts [17-19]. The administration of β -blockers is commonly performed prior to cardiac CTA. In addition sublingual nitroglycerin is often used for the dilation of the coronary artery lumen thus increase the number of evaluable segments. The main objective of the image quality improvement is to increase the diagnostic accuracy of CTA for the detection of CAD.

1.2 Prospectively ECG-triggered image acquisition

Radiation exposure is a major concern in coronary CTA. A multicenter (50 sites), observational study sought to estimate radiation dose in 1,965 patients undergoing coronary CTA. The median effective dose was 12 mSv [20]. Comparatively, invasive coronary angiography effective dose values ranges from approximately 5 to 7 mSv [21, 22]. When interpreting coronary CTA, data is acquired with either helical (also known as spiral) or axial scan mode. In helical image acquisition the gantry is continuously rotating while the patient table smoothly moves through. In contrary during axial scan mode the x-ray tube and detector system must complete a full (360-degree) or partial (180-degree) rotation around the patient while the patient table is stationary. The table moves incrementally along the z-axis (also known as pitch) to collect data [23]. Synchronization of axial scanning with the cardiac cycle is achieved by using the ECG signal. During prospectively-ECG triggered or also known as “step and shoot” scan image acquisition is initiated after the detection of the R-peak and data is obtained within a predefined-phase of the R-R interval. While the table moves to the next z-axis position radiation exposure is suspended. This “step” then repeats until the entire heart is covered. Images acquired with this method can be reconstructed within a pre-specified period of the cardiac cycle. Prospectively-ECG triggered scans permit data acquisition at doses of 1-6 mSv [24-26]. Newer developments on CT systems allow prospectively-ECG triggered helical scanning with high pitch values, thus providing ultra-low-dose image acquisition (<1 mSv) [27].

In the multivendor PROTECTION III study image quality of patients with prospectively-ECG triggered axial scan protocol was not inferior to helical scan protocols (subjective image score 3.36 ± 0.59 vs. 3.37 ± 0.59 , $p=0.866$), and the use of axial scan protocols resulted in a 70% radiation dose reduction (3.5 ± 2.1 mSv vs. 11.2 ± 5.9 mSv, $p<0.001$) [16]. However, images obtained with this method are more prone to cardiac motion artifacts, therefore patients undergoing this scan technique have to be carefully selected. A prerequisite to achieve diagnostic image quality is the stable or low HR with a suggested cut-off of <65 bpm and optimally <60 bpm [6, 16, 28, 29]. Hence coronary CTA is customarily performed in selected patients with favorable HR and rhythms, and premedication is often required to induce bradycardia, usually via blockade of beta-adrenergic receptors.

1.3 Diastolic and systolic acquisition with absolute and relative delay

CTA image acquisitions are typically performed in the most quiescent period of the cardiac cycle during mid-diastole [3, 30]. While the duration of this period is relatively lengthy and predictable in patients with low and stable HR, at higher HRs the length of diastasis significantly shortens and eventually disappears [31]. Alternatively, the end-systolic phase is the second relatively quiet phase where data acquisition is suitable [32]. This period is also less sensitive to R-R variability and arrhythmia as compared to diastole [30, 33]. For example, the length of systole shortens by 5.6 % as HRs increase from 80 to 90 bpm, while at the same time the length of diastole decreases by 16.4 % [34]. Thorough investigations have established that image reconstruction using diastolic data is favorable at HRs under 65 bpm [3, 4, 35], while at increased HRs, the end-systolic and early-diastolic reconstructions are more favorable [4, 36, 37]. Furthermore, the length of systole is a relatively fixed phenomenon, and end-systole can be targeted by using absolute delay times, as opposed to defining the timing of systole as a fraction of the cardiac cycle.

In cardiac CTA, several image reconstruction algorithms related to ECG signal can be utilized to obtain diagnostic image quality [38]. Typically images are reconstructed during the least motion or between T and P waves. The most frequently used approach is the relative delay method, in which the reconstruction starts after a certain delay from the prior wave which is ascribed as a certain percentage of the R-R interval. Another method is the absolute delay method in which reconstruction starts at a fixed time delay before or after the R wave and is ascribed as a specific time delay in milliseconds [39]. Of note, comparisons of the two image reconstruction techniques have been infrequently investigated.

1.4 Premedication before coronary CTA

Metoprolol is the IV β -blocker of choice for HR lowering in patients undergoing coronary CTA [7-9]. β -blockers are safe and efficacious in most patients, but contraindications such as reactive airway disease and hypotension are occasionally a serious challenge [7]. However, a previous survey revealed that 50% of centers allow an HR of more than 70 bpm for coronary CTA, mainly because of concerns regarding potential side effects of β -blocker administration [40]. The half-life of IV metoprolol is approximately 3 to 7 hours; therefore, if adverse effect occurs as a result of the HR-lowering, it may debilitate the patient for hours. These data indicate the need for a safe, short-lasting HR control. Esmolol is a cardioselective IV β -blocker with a rapid onset (within 2-3 minutes) and ultrashort duration of action (mean half-life [t_{1/2}] = 9 minutes) [41]. The rapid onset and offset of effects of esmolol provide an element of safety not previously available with longer-acting β -blockers [42]. However, no direct comparison between esmolol vs. metoprolol for HR control during coronary CTA is available.

Nitroglycerine is frequently used alongside β -blockers for rapid dilation of the coronary arteries. Nitroglycerin is routinely administered to alleviate the discomfort of angina and has a half-life of about 5 minutes [43, 44]. The administration of sublingual nitroglycerin during coronary CTA improves the evaluation of coronary segments, in particular, in smaller coronary branches as well as provides better image quality and improved diagnostic accuracy. A comprehensive systematic review on the use of sublingual nitroglycerine in coronary CTA suggests that the optimal starting time for image acquisition is probably between 3 and 4 minutes after sublingual administration of nitroglycerin [45]. Sublingual spray is superior to the sublingual tablet as it is more efficacious and is associated with fewer side effects [46, 47]. The most common side effects are headache and dizziness, which are typically the consequence of nitrate-induced hypotension [47, 48]. A compensatory mechanism for nitrate-induced hypotension is the increase of HR, which might hamper the image acquisition. Available data is controversial regarding HR changes after the administration of sublingual nitroglycerine. Some of the previous studies found no significant HR/blood pressure (BP) changes [49-51] while others reported substantial increase in HR [52, 53].

1.5 Anatomy of the aortic root

The aortic root originates from the basal attachments of the aortic valve leaflets within the left ventricular outflow tract (LVOT) and extends cranially to the sinotubular junction. It surrounds and supports the aortic valve and functions as a transition zone where the ventricular structure changes into fibroelastic tissue of the aortic trunk. The aortic root is a geometrically complex structure, which includes the annulus, the semilunar aortic leaflets, the interleaflet triangles, the sinus of Valsalva, and the sinotubular junction [54, 55]. There are three dilations (sinuses) in the wall of the aortic root just superior to the semilunar leaflets. Two of the three sinuses give rise to the coronary arteries (**Figure 3**).

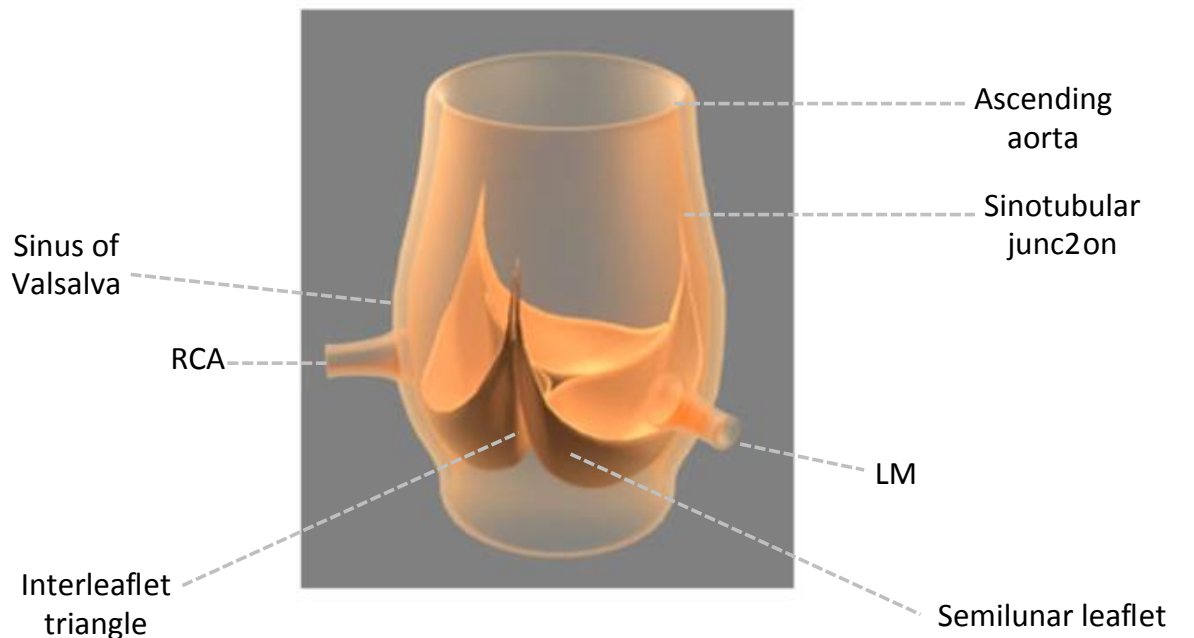


Figure 3. Aortic root with aortic valve on the inside [56]

The three valve leaflets are connected to the inner wall of the aorta creating the interleaflet triangles. Two of the three sinuses give rise to the origin of the left main (LM) and right coronary artery (RCA).

The annulus is not a true anatomical entity but is a virtual ring defined by the lowest insertion points (i.e. hinge points) of the three aortic leaflets (**Figure 4**).

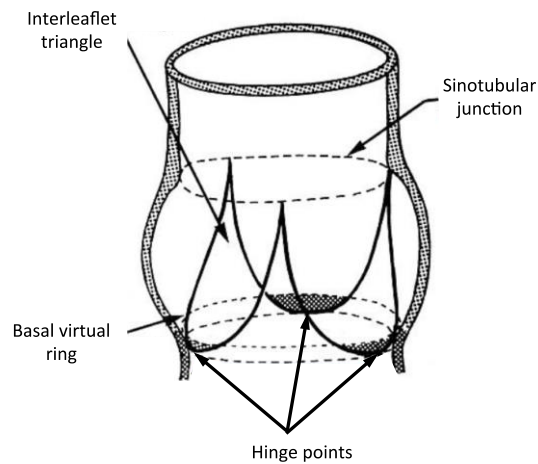


Figure 4. Aortic root with the virtual ring of the annulus [57]

Annulus defined as a virtual ring formed by the 3 lowest insertion points (i.e. hinge points).

When obtaining aortic root measurements with transthoracic echocardiography (TTE) the following dimensions are recorded: the annulus, diameter of the sinus of Valsalva, diameter of the sinotubular junction and diameter of the proximal ascending aorta (**Figure 5**).

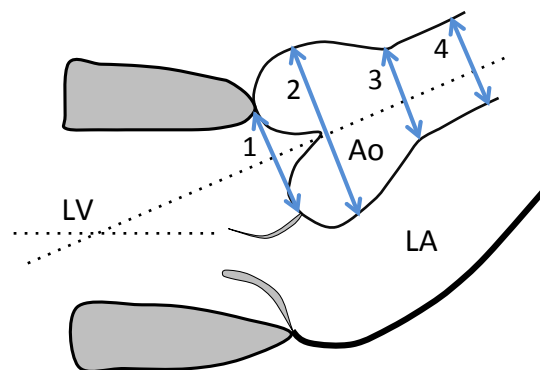


Figure 5. Aortic root measurements by TTE [58]

1. annulus; 2. sinus of Valsalva; 3. sinotubular junction; 4. ascending aorta; LV: left ventricle; LA: left atrium; Ao: aorta. Dashed lines depicting the longitudinal axes of the LV and of the aortic root.

1.6 CTA for the assessment of the aortic root

The aortic root is a complex anatomical structure therefore its 3D imaging is of paramount importance. CTA provides isotropic data, which can be reconstructed in any 3D imaging plane.

The annulus is the tightest part of the aortic root and is defined as a virtual ring formed by the 3 lowest points (i.e. hinge points) of the aortic leaflets as they connect to the wall of the LVOT [55]. A post-mortem study revealed that the shape of the annulus is not circular but rather oval [59]. 2D measurements (e.g. 2D TTE) of the annulus are therefore limited as they are based on a single plane, assuming a circular plane of the annulus. However, CTA-based findings are in line with autopsy findings, and suggest, that the annulus has an oval configuration in approximately 50% of patients evaluated for TAVI procedure, with a mean difference of 2.9 ± 1.8 mm between coronal and sagittal views [60]. Another CTA study reported an oval shape of the annulus in 91% of patients [61]. These differences might be attributable to the methodology used for image analysis. Previously, during CTA measurement of the aortic root, short (D_S) and long (D_L) diameters of the annulus were measured on the coronal and sagittal views, which roughly correspond to long-axis or 3-chamber view on TTE. The disadvantage of this method was, that it did not provide a clearly defined plane, which is required to identify the true short and long diameters of the annulus. Precise diameters can be measured by manipulating other planes to create a double-oblique plane, which contains the 3 insertions points. When the plane has been obtained measurement of the short and long diameters is necessary to calculate the mean diameter (D) of the aortic annulus: $[D = (D_L + D_S)/2]$ [1]. The second important parameter, when measuring aortic annulus is the area (A) and calculation of the diameter that corresponds to this area under the assumption of full circularity: $[D = 2\sqrt{(A/\pi)}]$. The third measurement is the circumference (C) of the aortic annulus and calculation of the circumference-derived diameter: $(D = C/\pi)$ [1] (**Figure 6**). Besides the annulus, diameter of LVOT, sinus of Valsalva, sinotubular junction and ascending aorta can be precisely extracted from the CTA dataset (**Figure 7**).

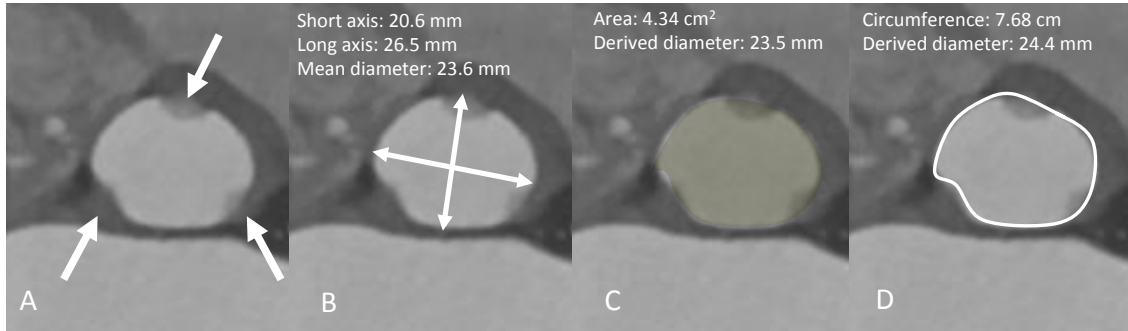


Figure 6. Assessment of the annulus dimensions by CTA (*own material*)

A: the 3 lowest insertion points of the aortic leaflets (white arrows); B: long and short diameter (left-right white arrows) and calculated mean diameter; C: area and area-derived diameter; D: circumference and derived diameter

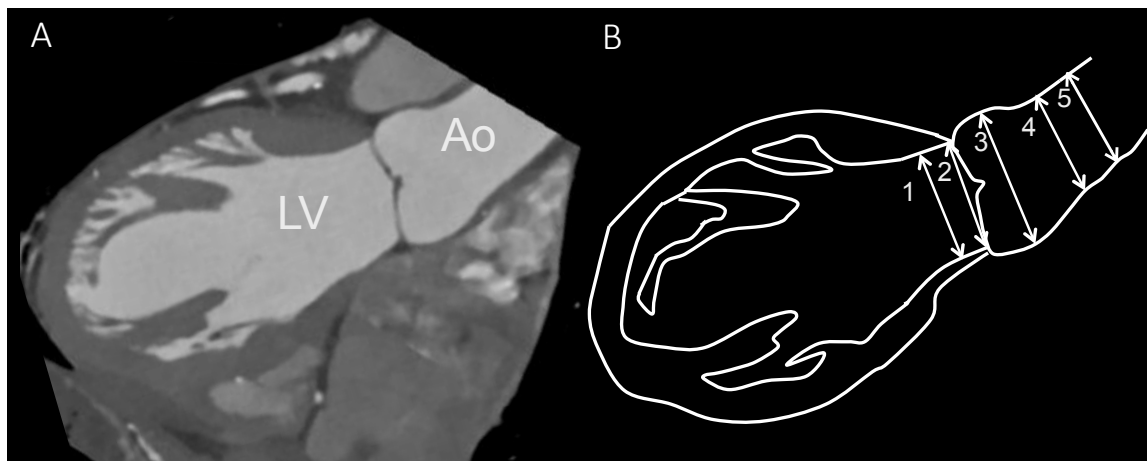


Figure 7. Relevant aortic root measurements by CTA (*own material*)

A: CTA image of the left ventricle (LV) and aorta (Ao); B: Outline of the LV and Ao with other relevant aortic root measurements: 1. left ventricular outflow tract; 2. annulus; 3. sinus of Valsalva; 4. sinotubular junction; 5. ascending aorta

1.7 Determinants of the aortic root geometry: genetics versus environment

The configuration of the aortic root is determined by genetic and environmental factors [62-66], however their respective contributions are still unclear. Assessment of genetic influence might help to identify subjects predisposed to future aortic root dilation. Previous studies examining the heritability of the aortic root diameter using TTE observed moderate genetic effect [63, 67], which indicates that a major proportion of phenotypic variance is due to environmental factors [63].

However, technical limitations of TTE can affect the accuracy of heritability estimates. Higher inter-reader variability of TTE versus CTA in the assessment of the annulus was previously demonstrated [68]. Furthermore, a retrospective comparison of aortic root dimensions by CTA and TTE demonstrated that TTE systematically underestimates the aortic root dimensions in patients with dilated aortic root [69]. Importantly, measurement errors artificially inflate the magnitude of environmental effects in heritability studies. Therefore, heritability estimates of the aortic root might be influenced by the measurement method. Precise measurements can provide more realistic estimates of genetic dependency.

Heritability estimates are frequently investigated among family studies which allow for the estimation of the risk for the disorder in relatives. However, their drawback is that the estimate of risk may include both genetic and environmental influences. As twins share environmental factors to a unique degree [70], environmental confounders are minimized and the role of genetic influence can be well investigated.

Environmental factors are also crucial in defining phenotypes. Results of the Framingham Heart Study concluded that age, height, weight and sex are the principal determinants of aortic root diameters [71]. Several investigations examined the effect of hypertension over the aortic root [65, 66, 71], however its association with the enlargement of aortic metrics is still unclear [66, 72]. A recent meta-analysis found no direct association between BP values and aortic root size [66]. Therefore equipoise remains on the impact of hypertension on aortic root dimensions.

2. OBJECTIVES

2.1 Defining the optimal systolic phase targets by using absolute delay

Coronary artery motion and deformation during cardiac cycle lead to significant motion artifacts when velocity of the coronaries exceeds the temporal resolution of the CT scanner. Furthermore, diastolic image acquisition might not be sufficient in patients with higher and/or variable HR. Therefore we aimed to determine the optimal systolic phase targets based on the velocity of the coronary arteries in patients at various HRs by using an absolute reconstruction delay time within the R-R interval.

2.2 Defining the efficacy and safety of esmolol vs. metoprolol

Artifact-free images are of importance for the diagnostic assessment of coronary arteries. Therefore adequate premedication of patients with higher HR prior to coronary CTA is recommended. The most common approach is the administration of IV metoprolol, however potential side-effects might hamper its application. Our aim was to investigate whether ultrashort half-life esmolol is at least as efficacious as the standard of care IV metoprolol for HR reduction during coronary CTA. We also sought to estimate the incidence of bradycardia (defined as HR <50 bpm) or hypotension (defined as systolic BP <100 mm Hg) as an effect of β -blockers in the esmolol and metoprolol groups.

2.3 Defining the heritability of the aortic root by CTA and TTE

2D and 3D imaging of the aortic root often show measurement discrepancies. Therefore, heritability estimates of aortic root dimensions can also vary upon the measurement method. We sought to assess the extent of heritability of the aortic root dimensions with the use of CTA in monozygotic (MZ) and dizygotic (DZ) twins. Furthermore, we aimed to derive TTE-based heritability estimates and compare these with the CTA based results.

3. METHODS

3.1 Study design and study population for optimal systolic phase

This retrospective cohort study consisted of 21 selected patients (14 men, 7 women; mean age 53.6 years \pm 13.1; age range, 29-78 years) who were referred for clinically indicated coronary CTA between November 2012 and May 2013 at the Department of Radiology, Massachusetts General Hospital. Patient selection was based on a clinical decision to target a systolic image reconstruction time interval (from at least 200-420 ms). None of the selected patients had coronary anomalies, nor had undergone coronary artery bypass grafting or prior electrophysiological interventions (such as ablation procedures, pacemaker implantation, or defibrillator implantation). Patients were divided into three groups based on mean HR (<65; 65-80; or >80 bpm). The mean HR was 71 bpm (range 52-96 bpm). The study was approved by the human research committee of the institutional review board (IRB), and compliance with the Health Insurance. A waiver of consent was obtained from our local IRB for this retrospective study.

3.1.1 Coronary CTA data acquisition and image analysis

All examinations were performed on a second-generation dual-source 128-slice CT scanner (SOMATOM Definition Flash, Siemens Medical Systems, Forchheim, Germany) with the following acquisition parameters: 128 slices at 0.6 mm thickness (using a z-axis flying focal spot) and gantry rotation time of 280 ms (and resultant temporal resolution of 75 ms). Tube potential (kilovolt-kV) and tube current (milliamperes-second-mAs) were calculated by an automatic tube potential selection algorithm based on antero-posterior scout image characteristics (CAREdose 4D and CAREkV, Siemens) [73]. Prospectively ECG-triggered axial-sequential acquisition (Sequential Scanning; Siemens) with an advanced arrhythmia rejection algorithm mode (Adaptive Cardio Sequence, “Adaptive Cardio Sequential Flex mode”, Siemens) was used in 18 scans, which enabled to reject and reacquire data at table positions scanned during heartbeats falling outside of a pre-specified cardiac cycle length. Systolic acquisition was performed using an absolute delay of 200-460 ms after the R-wave with peak (100 % of prescribed reference) tube current from 300 to 400 ms and a baseline plateau (20 % of the reference tube current) in the other prescribed phases [74].

Three patients underwent retrospectively ECG-gated CTA with peak targets in the same phases of systole and with aggressive (“MinDose”, Siemens) tube modulation outside of the 200-460 ms window. Raw datasets were reconstructed in 20 ms increments between 200 to 460 ms after the R peak using 1 mm thick slices and archived at the picture archival and communication system (PACS). Images were retrieved and displayed on a 3D workstation (Osirix v. 3.7.1 32-bit, Pixmeo, Geneva, Switzerland). Image review included axial source images, orthogonal and oblique MPR images, and thin slab MIP images, while advancing manually through the various acquired phases in 4-dimensional (cine) mode (**Figure 8**).

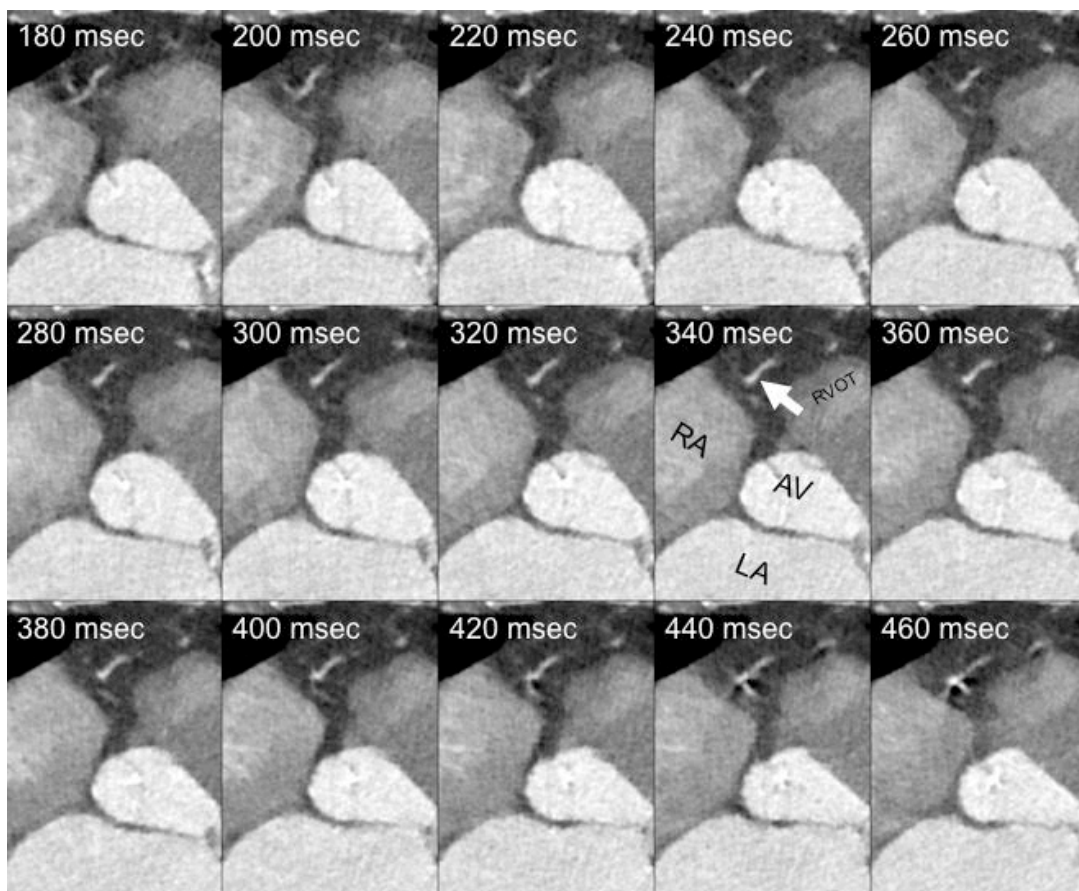


Figure 8. Raw dataset reconstructions in 20 ms increments after the R peak [75]

Multiple axial reconstructions of the right heart during systole (absolute delays after the R-wave from 180 ms through 460 ms, in 20 ms increments) demonstrate the optimal phase time of 340 ms at the level of the acute marginal branch (white arrow). RA: right atrium; LA: left atrium, AV: aortic valve; RVOT: right ventricular outflow tract

In patients without contraindications, 0.6 mg of sublingual nitroglycerine was administered approximately 5 min prior to scanning. Importantly, none of the patients received β -blockers during the examination, which was a decision at the discretion of the supervising CT physician as per standard site practice. However, 9 (43%) patients' home baseline regimen included oral β -blockers.

Arterial phase contrast was timed using the test bolus method using 20 ml iodinated contrast media (Iopamidol 370 g/cm³, Bracco Diagnostics Princeton, NJ USA) injected at a rate of 4-7 mL/s (based on body-mass index and IV access as per clinical routine) via an antecubital vein using a power injector. All injections were followed by a 40 ml of normal saline flush at a matching flow rate.

All scans were supervised by cardiovascular imaging specialists (at least one board-certified or eligible radiologist or cardiologist with advanced training in cardiac CT).

3.1.2 Coronary artery velocity mapping

Based on the SCCT coronary segmentation guidelines [12], six coronary artery landmarks, including the right coronary artery (RCA), first acute marginal branch (AM1), posterior descending artery (PDA), left main coronary artery (LM), first obtuse marginal branch (OM1), and second diagonal branch (D2) were identified in each patient, in 20 ms increments, by two experienced physicians.

The end systolic phase and the end of isovolumic relaxation phases were identified with the aortic valve closure and initiation of mitral valve opening on the three-chamber cine view as demonstrated in **Figure 9**.

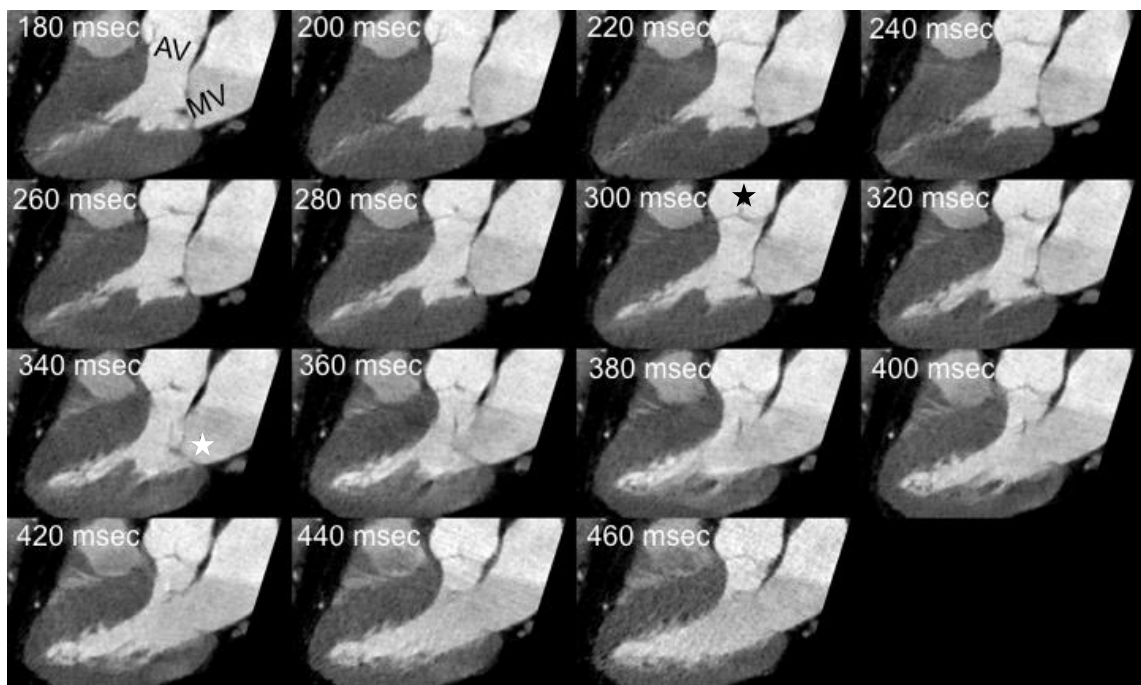


Figure 9. Defining the end systolic phase and the end of isovolumic relaxation on three-chamber cine view [75]

Images were reconstructed throughout the acquired systolic intervals and they demonstrating the aortic (AV) and mitral (MV) valve. Aortic valve closure (black asterisk at 300 ms reconstruction) and the initiation of mitral valve opening (white asterisk at 340 ms reconstruction) can be identified, which denote the end of the systolic reduced ejection phase, and the end of the isovolumic relaxation, respectively.

Coronary artery landmark position was traced manually by placing the cursor in the exact center of each landmark in every phase. The x, y and z-coordinates of the selected landmark were then recorded (**Figure 10**) and were used for the calculation of the 3D route of coronary artery motion by using a previously established method [15]. The velocity of the given landmark was defined as the quotient of the route and the length of the time interval, which was 20 ms.

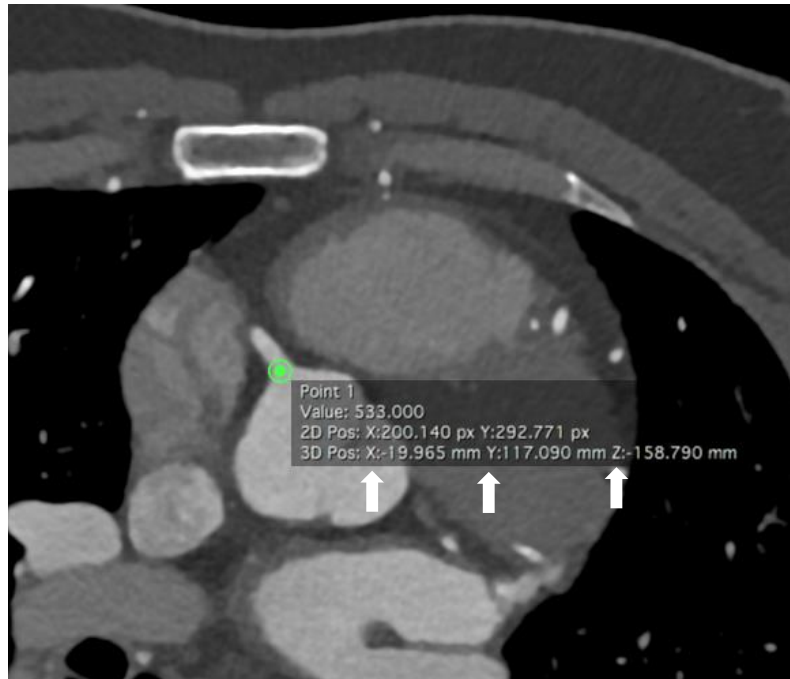


Figure 10. Axial CTA image of the heart with the origin of the RCA (*own material*) X, Y and Z (white arrows) indicate the coordinates of the RCA origin and are used for the calculation of the coronary artery velocity

To determine the optimal velocities in each coronary artery segment, the mean values of the minimum velocities were calculated separately for each HR group (i.e. <65; 65-80; and >80 bpm). The ideal reconstruction times in each HR group were defined as the R-R interval with the lowest minimum mean velocity in a given segment.

A preliminary analysis of 10 patients revealed that the mean lowest coronary artery velocities in each segment occurred in the middle (280-340 ms) of the selected time interval (200-460 ms). Therefore we divided this interval into three sections from: 200 to 260 ms (early), 280-340 ms (mid) and 360-420 ms (late), to observe if any significant difference existed between the three sections.

3.2 Study design and population for esmolol vs. metoprolol

Our study was a randomized single-center non-inferiority phase III clinical trial that compared two IV β -adrenergic receptor blockers to reduce HR in patients who underwent coronary CTA because of suspected CAD between April 2013 and September 2013 at Heart and Vascular Center, Semmelweis University. Subjects who had HR >65 bpm despite oral metoprolol pretreatment were enrolled in the study. Patients with history of a coronary intervention and an implanted stent with a diameter ≥ 3 mm or previous coronary artery bypass surgery were eligible to participate in the study [76]. Individuals with a HR other than sinus rhythm, any contraindication against β -blocker (asthma bronchiale, chronic obstructive pulmonary disease, any type of documented atrioventricular block, severe aortic valve stenosis, severe left ventricular dysfunction characterized by ejection fraction below 30%), or a systolic BP <100 mm Hg before the coronary CTA scan were excluded from the study. In total, 650 consecutive patients referred to coronary CTA were screened, and of these, 574 patients were eligible to participate in the study. In 162 patients no IV drug was administered because the HR before scan was ≤ 65 bpm. In total, 412 patients (with HR >65 bpm before the scan) were enrolled and randomized into either esmolol or metoprolol group; 204 patients received IV esmolol and 208 patients received IV metoprolol (**Figure 11**).

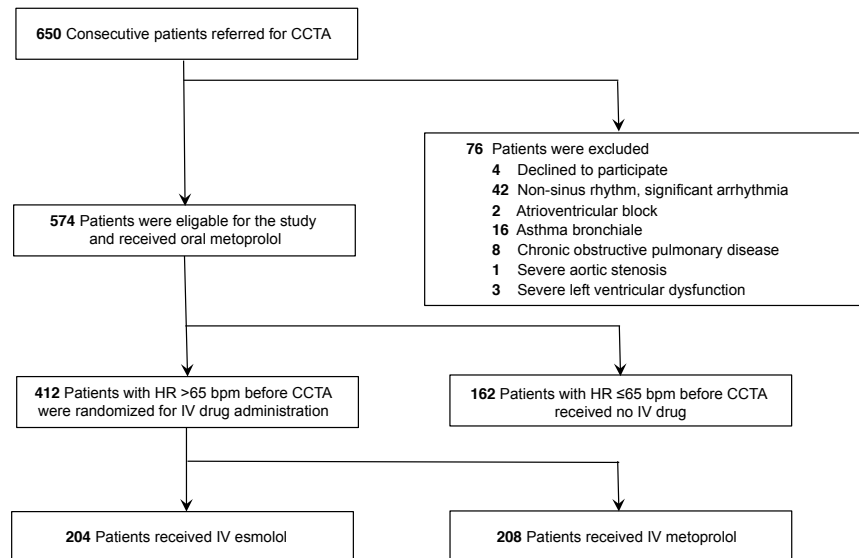


Figure 11. Flow chart of the study [77]

Bpm: Beat per minute; CCTA: coronary CT angiography; IV: intravenous; HR: heart rate

3.2.1 Drug administration protocol and heart rate monitoring

Patients received 50-mg oral metoprolol at arrival if the HR was >65 bpm. If the HR was ≥ 80 bpm, 100-mg oral metoprolol was administered. The HR was re-evaluated 60 minutes after the oral β -blockade, immediately before the coronary CTA examination. Patients presenting with HR >65 bpm on the CT table were randomized to IV esmolol or IV metoprolol administration. In both, the investigational (esmolol) and the active control (metoprolol) groups, the IV drug was administered by the physician performing the coronary CTA scan. To achieve randomization, we administered esmolol on even weeks and metoprolol on odd weeks in an alternating fashion. The IV metoprolol (Betaloc; 1 mg/mL; AstraZeneca, Luton, United Kingdom; 5-mg ampoule) was titrated in 5-mg doses in every 3 minutes until the target HR (≤ 65 bpm) or the maximum dose of metoprolol (20 mg) was achieved [78].

The esmolol (Esmocard; 2500 mg/10 mL; AOP Orphan Pharmaceuticals AG, Vienna, Austria) was diluted to 500 mg/10 mL and titrated in ascending 100-, 200-, 200-mg doses in every 3 minutes until the target HR (≤ 65 bpm) or the maximum dose of esmolol (500 mg) was achieved. BP was monitored before every administered drug bolus. If hypotension (defined as systolic BP <100 mm Hg) or bradycardia (defined as HR <50 bpm) was measured, the administration of the β -blocker agent was suspended. Two puffs of sublingual nitroglycerine were given to each patient 3 to 5 minutes before the CT scan to ensure the proper visualization of the coronaries. The HR was recorded at arrival (T1), immediately before coronary CTA (T2), during breath-hold, contrast injection, and scan (TS), immediately after scan (T3), and 30 minutes after coronary CTA scan (T4). BP was measured at T1, T2, T3, and T4 time points.

We have performed an interim analysis after 45 days to ensure adequate enrollment rate and to assess toxicity as well as adverse events. An adverse event was defined as a change in health condition resulting from the administration of β -blockers, which is not resolving with observation and requires medical intervention.

3.2.2 Coronary CTA scan protocol

CTA examinations were performed using a 256-slice multidetector-row CT (Brilliance iCT, Philips HealthTech, Best, The Netherlands) with the following acquisition parameters: 128 mm×0.625 mm collimation, 270 ms rotation time, 80-120 kV tube voltage, 150-300 mAs tube current depending on the patients' body mass index (BMI). Contrast-enhanced images were acquired using prospective ECG triggering at 75% to 81% phase (3% padding). The iodinated contrast agent (Iomeron 400; Bracco Ltd, Milan, Italy) was injected into an antecubital vein via an 18-ga cannula using a dual-syringe technique, at a flow rate of 3.5 to 5.5 mL/s depending on patients' BMI and the tube voltage. Bolus tracking was performed using a region of interest in the left atrium. Images were reconstructed with a slice thickness of 0.8 mm and 0.4 mm increment. CT datasets were analysed offline on workstations equipped with dedicated cardiac post-processing software (Intellispace Portal, Philips HealthTech).

3.3 Study design and population for heritability of the aortic root

Our study population consisted of 202 twins (61 monozygotic (MZ), 40 dizygotic (DZ) same-sex pairs), who were enrolled in the BUDAPEST-GLOBAL (Burden of atherosclerotic plaques study in twins - Genetic Loci and the Burden of Atherosclerotic Lesions) clinical study between April 2013 and July 2014, at Heart and Vascular Center, Semmelweis University. Detailed description of the study protocol has been published previously [79]. Briefly, the BUDAPEST-GLOBAL study is a prospective, single-center, classical twin study that sought to evaluate the influence of genetic and environmental factors on the burden of CAD. Participants with self-reported Caucasian ethnic background were enrolled from the Hungarian Twin Registry on a voluntary basis [80]. Two twin pairs were excluded from the CTA analysis due to insufficient image quality (one pair) and withdrawal of study consent (the other pair), while eight twin pairs were excluded from TTE analysis due to the poor quality of the acquired images. No subjects were excluded for the presence of severe valve disease. In total, 198 twin subjects were analysed by CTA and 186 by TTE. Complete physical examination and anthropometric measurements were performed in all participants, which included the recording of waist circumference, height and weight as well as the calculation of the BMI. Brachial blood pressure values were recorded prior to CTA. Traditional cardiovascular risk factors such as hypertension, diabetes mellitus, dyslipidaemia and smoking habits were collected from patients' medical history. All participants provided informed consent. The investigation was approved by the National Research Ethics Committee (IRB number 58401/2012/EKU [828/PI/12]; amendment: 12292/2013/EKU) and was conducted according to the principles stated in the Declaration of Helsinki.

3.3.1 CTA scan and drug administration protocol

All CTA examinations were performed using a 256-slice multidetector-row CT (Brilliance iCT, Philips HealthTech, Best, The Netherlands) with the following acquisition parameters: 128 mm×0.625 mm collimation, 270 ms rotation time, 100-120 kV tube voltage, 200-300 mAs tube current depending on the patients' BMI. Contrast-enhanced images were acquired using prospective ECG triggering at 78% phase (3% padding). If the initial heart rate of the participants was >65 bpm, oral (maximum dose of 100 mg) or intravenous (maximum dose of 20 mg) metoprolol was administered. Subjects received 0.8 mg of sublingual nitroglycerin, no more than 2 minutes before image acquisition. Triphasic contrast injection protocol was performed using 80 mL of iodinated contrast agent (Iomeprol 400 g/cm³, Iomeron, Bracco Imaging S.p.A., Milano, Italy), mixture of contrast agent and saline (10 mL contrast agent and 30 mL saline) and a chaser of 40 mL saline, all injected with a flow rate of 4.5-5.5 ml/s into an antecubital vein. Bolus tracking was performed using a region of interest in the left atrium. Images were reconstructed with a slice thickness of 0.8 mm and 0.4 mm increment. CT datasets were analysed offline on workstations equipped with dedicated cardiac post-processing software (Intellispace Portal, Philips HealthTech).

3.3.2 CTA analysis of the aortic root

The following diameters were measured by a single reader (CC, with three years of experience): left ventricular outflow tract (LVOT), annulus, sinus of Valsalva, sinotubular junction and ascending aorta (**Figure 12**).

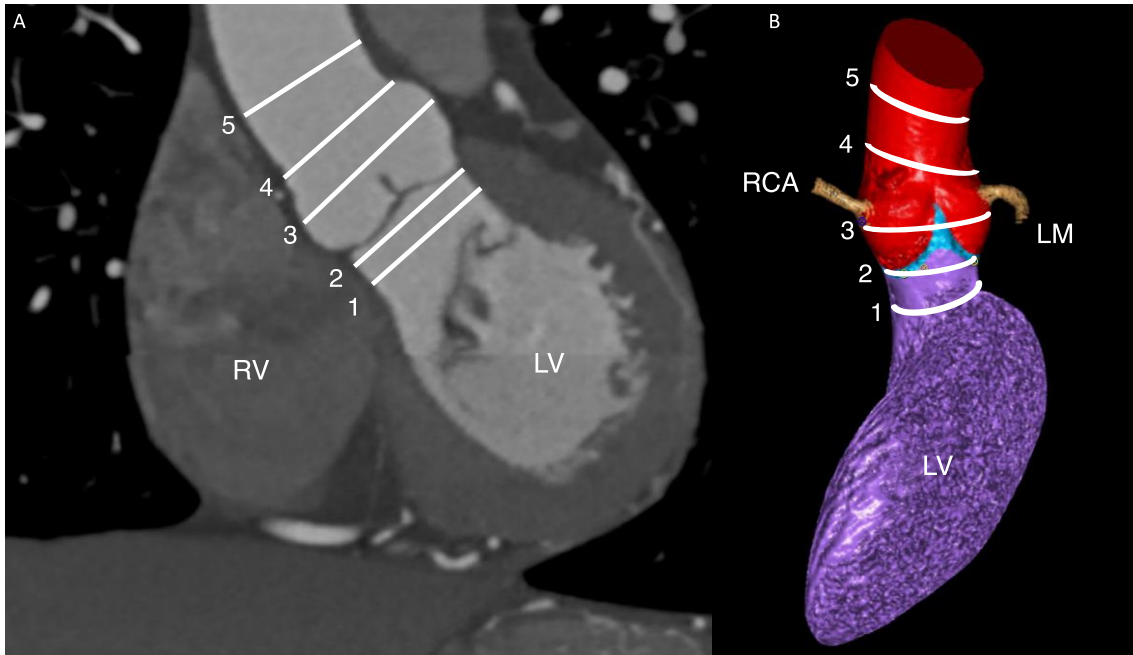


Figure 12. CTA-based aortic root measurements [81]

A: coronal CTA image of the left ventricle (LV), right ventricle (RV) and aortic root; B: 3D volume rendered image of the aortic root and the left ventricular cavity. White lines correspond to measured aortic root diameters: 1. left ventricular outflow tract; 2. annulus; 3. sinus of Valsalva; 4. sinotubular junction; 5. ascending aorta; LM: left main coronary artery; RCA: right coronary artery

By using a semi-automated software tool (Intellispace Portal, Philips HealthTech) modified orientation views similar to those used for TAVI procedures were acquired for the initial evaluation of the aortic root [1]. The axial plane was automatically aligned with the lowest insertion points of the 3 coronary cusps (**Figure 13**). In case of misalignment manual correction of the insertion points was performed. Based on the annulus-plane diameters of the LVOT, annulus, sinus of Valsalva, sinotubular junction and ascending aorta were obtained by the software. The diameter of a given structure was defined as the mean of the short and long axis [1]. To assess intra-reader reproducibility the same reader performed the previously described measurements in 20 twin pairs. For inter-reader reproducibility, another experienced reader (MK, with five years of experience) also measured the diameters of the aortic root. All measurements were performed blinded to the zygosity of twins.

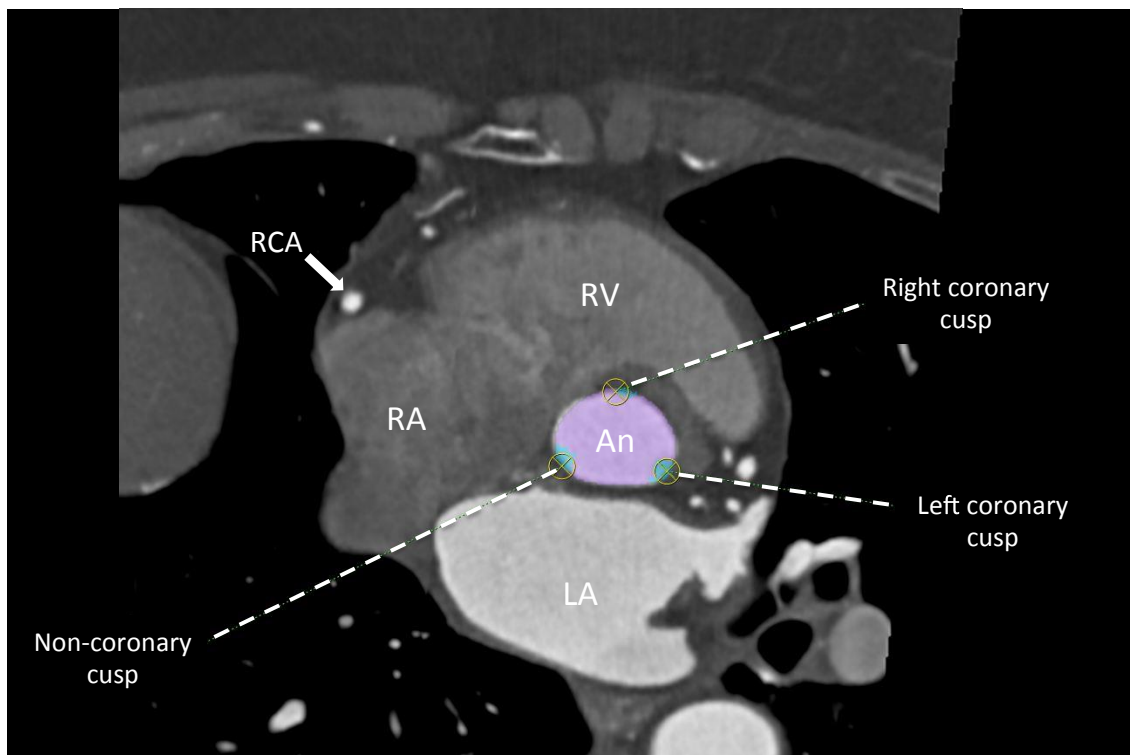


Figure 13. Axial plane of the annulus on CTA (*own material*)

Annulus defined by the three lowest insertion points (right coronary cusp, left coronary cusp and non-coronary cusp). An: annulus; LA: left atrium; RA: right atrium; RV: right ventricle; RCA: right coronary artery

3.3.3 TTE imaging of the aortic root

Two-dimensional TTE was performed using iE33 system, S5-1 transducer (Philips Healthcare, Best, The Netherlands). Aortic root measurements were obtained by one experienced operator (AK, with three-years of experience), who was blinded to the zygosity of the twins and the CTA exams. Standard two-dimensional protocol was used according to current guidelines [58]. Parasternal long-axis views were acquired to measure the LVOT and aortic root at the level of the annulus, sinus of Valsalva, sinotubular junction and ascending aorta using the inner edge to inner edge method (**Figure 14**) [58]. The LVOT and the annulus were measured in zoom mode. Diameters of the LVOT and annulus were assessed on a mid-systolic frame, all other parameters on end-diastolic frame [58]. All recordings included 3 cardiac cycles and were exported to a workstation for off-line analysis (Image-Com, TomTec Imaging Systems, Unterschleissheim, Germany). To assess intra-reader reproducibility the same reader performed the previously described measurements in 20 twin pairs. For inter-reader reproducibility, another experienced reader (AAM, with eight years of experience) also measured the diameters of the aortic root. Inter-modality agreement between CTA and TTE was also calculated.

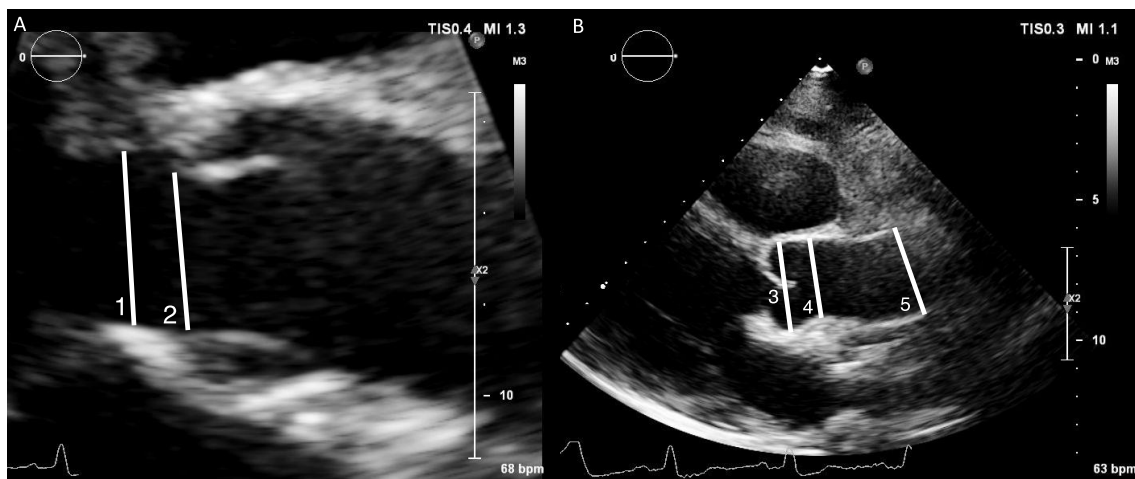


Figure 14. TTE-based aortic root measurements [81]

A: zoomed parasternal long-axis view at mid-systolic frame of the aortic root; B: optimized parasternal long-axis view at end-diastolic frame of the aortic root; Inner edge to inner edge method was applied. White lines correspond to measured aortic root diameters: 1. left ventricular outflow tract; 2. annulus; 3. sinus of Valsalva; 4. sinotubular junction; 5. ascending aorta

3.4 Statistical analyses

Continuous variables were reported as mean \pm standard deviation (SD) or median (interquartile range) for non-normally distributed data. Categorical variables are given as frequency (%). Normal distribution was tested using the Shapiro-Wilk tests. Non-parametric data was analyzed using robust *t* tests using 20%-trimmed means with bootstrapping or when data was very skewed applying a Mann–Whitney-U test. Differences of categorical variables between treatment groups were analyzed by chi-square tests. Correlations were calculated with Pearson's correlation test or Spearman's rho test as appropriate. To compare multiple variables one-way ANOVA, followed by Bonferroni post hoc test, or Kruskal–Wallis ANOVA followed by Mann–Whitney-U test was used depending on normality. Within subjects, measurements were compared using repeated measures ANOVA. A *P*-value of <0.05 was considered significant. Statistical analyses were performed with R, version 3.0.2 (R Foundation for Statistical Computing, Vienna, Austria).

3.4.1 Sample size calculation for the esmolol vs. metoprolol study

The sample size calculation to determine the efficacy and safety of esmolol was based on prior research, which showed that 83% of patients who received metoprolol premedication achieved a HR of ≤ 65 bpm [82]. The non-inferiority margin was set to 10% because we have assumed that this is a clinically acceptable maximum difference between the responder proportions of the two treatment groups. Thus, our primary aim to achieve at least 73% responder proportion seemed to be realistic. A total of 595 patients, 297/298 patients on each treatment arm, were needed to find a difference between proportions of responders in metoprolol group vs. esmolol group. The sample size calculation was based on an intention to treat analysis using a non-inferiority margin set at 10% with a power of 90%. Dedicated software was used for sample size calculation (East, version 5.4.1; Cytel Inc, Cambridge, Massachusetts).

3.4.2 Statistical analysis for heritability estimates

Based on CTA and TTE measurements we determined co-twin correlations between MZ and DZ twins. In addition to correlation-based similarities a structural equation model, the ACDE model was used to decompose the total variance between twins. In the ACDE model four latent variables: additive genetic (A), common environmental (C), dominant genetic (D) and unique environmental (E) effects drive the variance of phenotype in each twin. Since C and D factors are confounded only models calculating with C or D, next to A and E can be used. Additive genetic effects (A) are perfectly (1.0) correlated across MZ twins and 0.5 correlated across DZ twins. Common environmental effects (C) are perfectly correlated within twin pairs independently of zygosity. Unique environmental effects (E) are uncorrelated within co-twins (**Figure 15**). Since measurement error in the phenotype is also uncorrelated across measurements, it appears as part of the unique environmental (E) component.

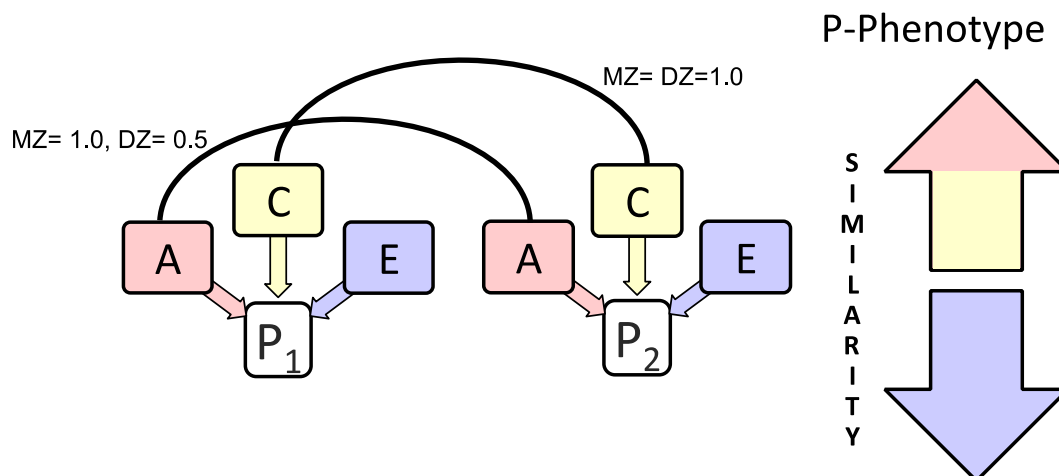


Figure 15. ACE model (*own material*)

Additive genetic effects (A) are perfectly (1.0) correlated across MZ twins and 0.5 correlated across DZ twins. Common environmental effects (C) are perfectly correlated within twin pairs independently of zygosity. Unique environmental effects (E) are uncorrelated within twins. Additive genetic effects (A) and common environmental effects (C) increase, while unique environmental effects (E) decrease the similarity between twins. P: phenotype

Statistical analyses were done using the R environment (version: 3.2.1) [83]. Two-sample t-test and chi-square test was used to assess differences between the measured parameters of MZ and DZ twins. Paired t-test was used to evaluate the differences between aortic parameters measured by CTA and TTE. Intra-and inter-reader variability was assessed using the intraclass correlation coefficient (ICC) using IRR package (version: 0.84) [84].

Structural equation modelling was used to decompose sources of variation using univariate ACDE models using the OpenMx package (version: 2.2.4) [85, 86]. Total variation between twins is considered to be a product of additive genetic (A), common environmental (C), dominant genetic (D) and unique environmental (E) effects. All factors cannot be simultaneously estimated since C and D are confounded due to statistical power issues, thus ACE and ADE models were calculated separately. Potential covariates were selected using all subset regression analysis using the leaps package (version: 2.9) [87]. Based on the results age, sex, height and diastolic blood pressure were included as covariates. Akaike Information Criterion (AIC) and Bayesian Information Criterion (BIC) were used to determine the most parsimonious model among calculated full models. Likelihood ratio test was used to assess the fit of the submodels compared to corresponding full models. In case the fit did not decrease significantly, the more parsimonious submodel was selected. Bootstrapped confidence intervals (CI) of all modelled parameters were calculated using 2000 iterations to achieve robust results.

4. RESULTS

4.1 Optimal systolic phase targets by using absolute delay

To define the optimal systolic phase targets at patients with various HR, we analyzed a total of 1488 coronary artery landmarks (24 of the various landmark data points were deemed non-evaluable or missing), in 21 patients at 6 locations throughout the coronary artery tree, at 12 time-points throughout the systolic phase reconstructions.

Overall, no correlation was found between coronary artery velocities and HR (RCA: $r=-0.08$, $p=0.75$; AM1: $r=-0.48$, $p=0.03$; PDA: $r=-0.31$, $p=0.17$; LM: $r=-0.14$; $p=0.54$; OM1: $r=-0.17$, $p=0.45$; D2: $r=-0.16$, $p=0.48$). **Table 1** lists the minimal velocities in millimeter/second (mm/s) in each segment for each HR group. No differences were found in the minimal coronary artery velocities between the three HR groups, with the exception of the AM1 branch ($p=0.005$) between <65 vs. >80 bpm ($p=0.03$), and at HRs of $65-80$ vs. >80 bpm ($p=0.006$).

Table 1. Minimal velocities across the coronary arteries in mm/s in each HR group [75]

RCA: right coronary artery; AM1: first acute marginal branch; PDA: posterior descending artery; LM: left main coronary artery; OM1: first obtuse marginal branch; D2: second diagonal branch

	<65	65-80	>80	All	<i>p</i>
RCA	14.2	12.4	12.6	13.1	0.880
AM1	19.5	21.9	9.4	16.9	0.005
PDA	22.1	15.8	15.0	17.7	0.413
LM	12.9	11.9	11.5	12.1	0.940
OM1	14.0	13.8	11.8	13.2	0.774
D2	14.1	12.6	12.7	13.1	0.884

Table 2 shows the optimal systolic phase reconstruction times of the evaluated coronary artery segments in milliseconds (ms). Significant differences in optimal reconstruction time points were detected only in the RCA ($p=0.019$) between HR of 65-80 bpm vs. >80 bpm.

Table 2. Optimal systolic phase reconstruction time in ms in each HR group

RCA: right coronary artery; AM1: first acute marginal branch; PDA: posterior descending artery; LM: left main coronary artery; OM1: first obtuse marginal branch; D2: second diagonal branch

	<65	65-80	>80	All	<i>p</i>
RCA	326	357	269	317	0.019
AM1	343	311	334	329	0.451
PDA	326	274	277	292	0.177
LM	300	263	257	273	0.249
OM	311	343	289	314	0.294
D2	277	306	303	295	0.542

Tables 1 and 2 indicate that coronary artery minimal velocities and optimal time-points are independent of HR. However, note that in two segments (AM1 and RCA) significant differences were demonstrated.

A preliminary analysis of ten patients revealed that the mean lowest coronary artery velocities in each segment occurred in the mid period (280-340 ms) of the acquired systolic phase (200-420 ms). Therefore we divided this interval into three time-periods from: 200 to 260 ms (early), 280-340 ms (mid) and 360-420 ms (late), to evaluate potential differences. The analysis of all 21 patients' mean velocities in each of the three time periods confirmed this observation. In the mid period, (280-340 ms) in each coronary segment, the mean velocity values were significantly lower versus the early and/or late phases of the selected time interval (**Table 3, Figure 16**). In the LM, OM1 and D2, a significant difference was also found between the early and late time periods.

Table 3. Differences between the systolic phase targets

RCA: right coronary artery; AM1: first acute marginal branch; PDA: posterior descending artery; LM: left main coronary artery; OM1: first obtuse marginal branch; D2: second diagonal branch

Coronary artery segment	Time interval (ms)	Mean velocity (mm/s)	<i>p</i> -value	<i>p</i> between time intervals
RCA	early (200 - 260)	48.4		
	mid (280 - 340)	44.6		mid vs. late
	late (360 - 420)	58.9		<i>p</i> =0.005
<i>p</i> =0.005				
AM1	early (200 - 260)	75.0		
	mid (280 - 340)	54.0		mid vs. early
	late (360 - 420)	66.4		<i>p</i> =0.004
<i>p</i> =0.005				
PDA	early (200 - 260)	79.2		
	mid (280 - 340)	51.5		mid vs. early
	late (360 - 420)	95.6		<i>p</i> =0.016
<i>p</i> <0.001				
LM	early (200 - 260)	41.4		
	mid (280 - 340)	41.1		mid vs. late
	late (360 - 420)	53.8		<i>p</i> <0.002
<i>p</i> <0.001				
OM1	early (200 - 260)	48.4		
	mid (280 - 340)	42.9		early vs. late
	late (360 - 420)	70.2		<i>p</i> =0.002
<i>p</i> <0.001				
D2	early (200 - 260)	42.0		
	mid (280 - 340)	42.6		mid vs. late
	late (360 - 420)	56.0		<i>p</i> =0.010
<i>p</i> =0.003				

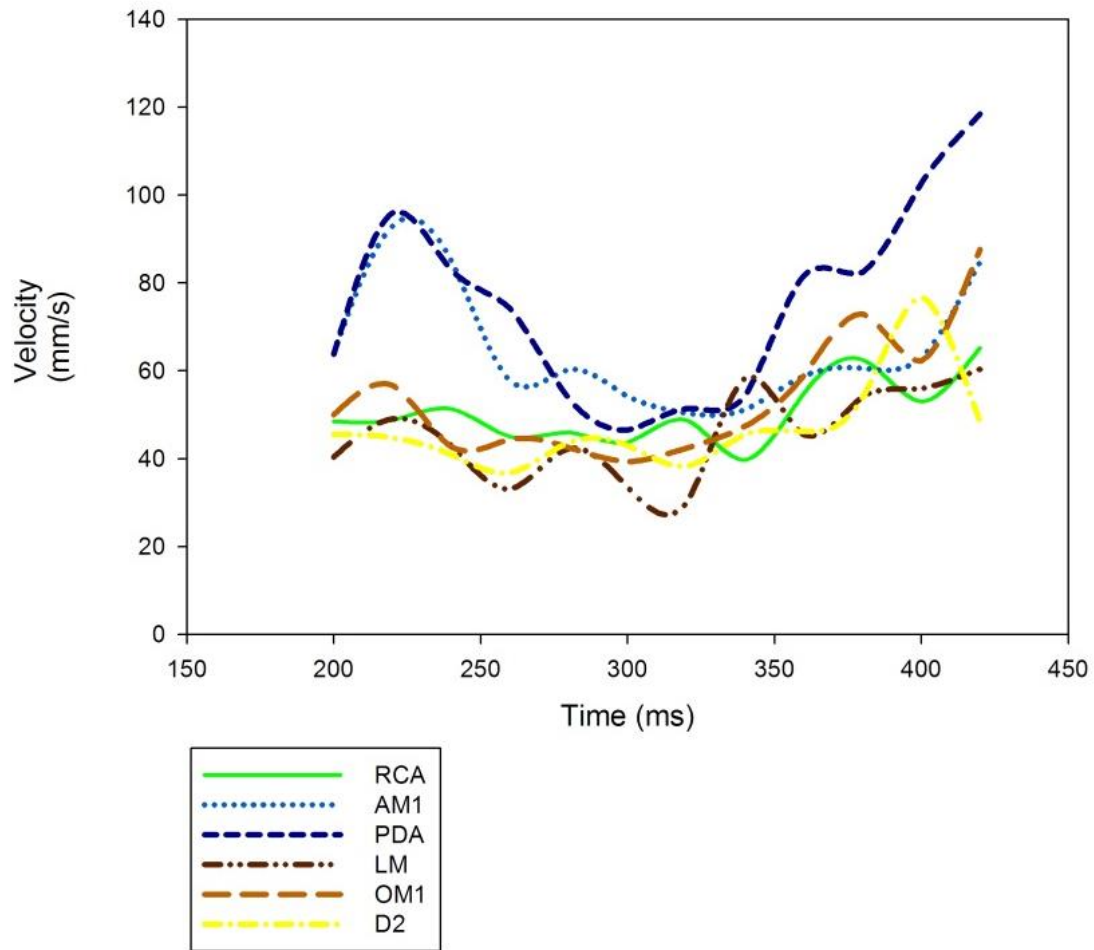


Figure 16. Mean coronary artery velocities in each of the three time periods [75]
The lowest coronary velocity was detected in the mid period (280-340 ms) of the reconstructed interval (200-420 ms). The mean velocities in this period were significantly lower than in the early and/or late periods.

4.2 Efficacy and safety of esmolol vs. metoprolol

Patient enrollment was terminated as early as the interim analysis indicated that IV esmolol is clearly non-inferior to IV metoprolol, and in fact, esmolol showed superior characteristics compared to IV metoprolol in reducing HR during coronary CTA.

There was no difference between the esmolol and metoprolol group regarding the clinical characteristics of patients (**Table 4**).

Table 4. Demographic characteristics of the study groups [77]

AMI: acute myocardial infarction; BMI: body mass index; CABG: coronary artery bypass graft; PAD: peripheral arterial disease; PCI: percutaneous coronary intervention; mean values \pm SD

	esmolol (n=204)	metoprolol (n=208)	<i>p</i>
age (years)	56.9 \pm 10.8	57.6 \pm 12.2	0.390
male/female	100/104	111/97	0.377
BMI (kg/m ²)	28.4 \pm 4.9	28.2 \pm 4.7	0.956
hypertension (%)	67	66	0.889
diabetes (%)	16	14	0.603
dyslipidemia (%)	48	55	0.154
AMI (%)	5	10	0.076
PCI (%)	5	7	0.455
CABG (%)	4	6	0.287
PAD (%)	9	8	0.801
stroke (%)	4	1	0.072
smoking (%)	25	26	0.845
β -blocker (%)	47	48	0.795

In the esmolol group, 53 of 204 patients (26.0%) received 1 bolus (100 mg), 73 of 204 (35.8%) received 2 boluses (300 mg), and 78 of 204 (38.2%) received 3 boluses (500 mg) of esmolol. In the metoprolol group, IV metoprolol was administered in a similar fashion as in the esmolol group but in 5-mg increments. Eighty-three of 208 patients (39.9%) received 1 bolus (5 mg), 45 of 208 patients (21.6%) 2 boluses (10 mg), 53 of 208 (25.5%) 3 boluses (15 mg), and 27 of 208 (13.0%) 4 boluses (20 mg) of metoprolol. Oral metoprolol administration was similar in the esmolol and metoprolol groups (51.2 ± 33.1 vs. 52.4 ± 33.6 ; $p=0.71$). On average, 325.6 ± 158.4 mg IV esmolol and 10.7 ± 6.3 mg IV metoprolol were administered. The mean HR of the esmolol and metoprolol groups was similar at the time of arrival (T1: 78 ± 13 vs. 77 ± 12 bpm; $p=0.65$) and immediately before the coronary CTA examination (T2: 68 ± 7 vs. 69 ± 7 bpm; $p=0.60$). However, HR during the scan was significantly lower among the patients who received IV esmolol vs. patients who received IV metoprolol (TS: 58 ± 6 vs. 61 ± 7 bpm; $p<0.0001$). On the other hand, HR immediately after the coronary CTA and 30 minutes after the coronary CTA was higher in the esmolol group than in the metoprolol group (T3: 68 ± 7 vs. 66 ± 7 bpm; $p<0.01$; and T4: 65 ± 8 vs. 63 ± 8 bpm; $p<0.0001$, respectively; **Table 5, Figure 17**). Systolic and diastolic BP showed no difference between the 2 groups measured at any time point (**Table 6**).

Table 5. Mean HR in the esmolol and metoprolol group

T1: arrival; T2: before scan; TS: during scan; T3: after scan; T4: emission; mean values \pm SD

	esmolol (n=204)	metoprolol (n=208)	<i>p</i>
T1	78 ± 13	77 ± 12	0.652
T2	68 ± 7	69 ± 7	0.599
TS	58 ± 6	61 ± 7	<0.0001
T3	68 ± 7	66 ± 7	<0.01
T4	65 ± 8	63 ± 8	<0.0001

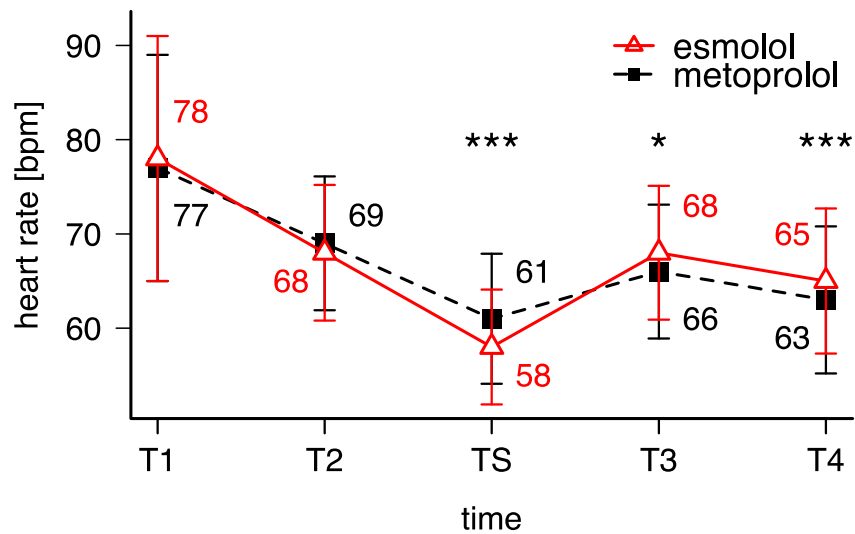


Figure 17. Mean HR in the esmolol and metoprolol group [77]

The figure represents the mean HR and their standard deviations in the esmolol and metoprolol groups at different time points. The red triangles represent the mean HR in the esmolol group, whereas the black squares indicate the mean HR in the metoprolol group. T1: time of arrival; T2: time point before the coronary CT angiography (CTA) scan; TS: during the coronary CTA scan; T3: time point immediately after the coronary CTA; T4: 30 minutes after the coronary CTA. * $p < 0.01$; *** $p < 0.0001$.

Table 6. Blood pressure in mm Hg in the esmolol and metoprolol group

T1: arrival; T2: before scan; T3: after scan; T4: emission; mean values \pm SD

	esmolol (n=204)	metoprolol (n=208)	<i>p</i>
T1			
systole	142 \pm 22	146 \pm 21	0.195
diastole	87 \pm 12	87 \pm 12	0.819
T2			
systole	144 \pm 21	145 \pm 20	0.918
diastole	86 \pm 13	87 \pm 12	0.945
T3			
systole	128 \pm 20	131 \pm 19	0.053
diastole	74 \pm 12	75 \pm 12	0.522
T4			
systole	132 \pm 20	134 \pm 21	0.414
diastole	79 \pm 11	80 \pm 12	0.589

HR of ≤ 65 bpm was reached in 182 of 204 (89%) patients in the esmolol group vs. in 162 of 208 (78%) patients in the metoprolol group ($p < 0.05$), whereas HR ≤ 60 bpm was reached in 147 of 204 (72%) patients who received esmolol vs. in 117 of 208 (56%) patients who received metoprolol ($p < 0.001$; **Figure 18**).

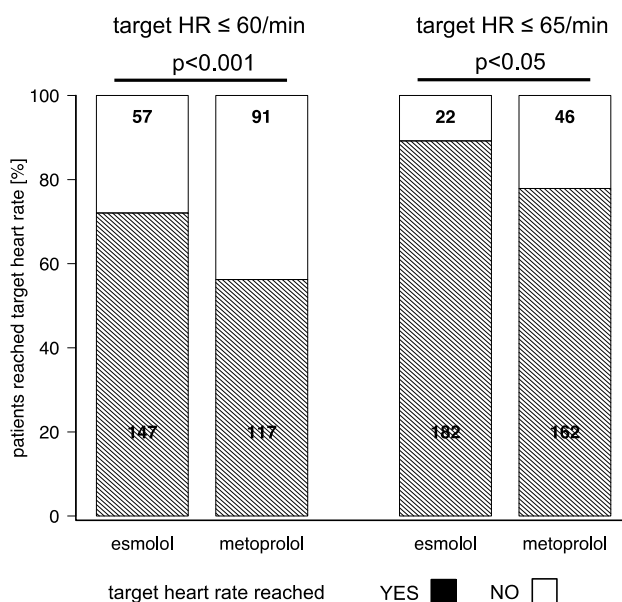


Figure 18. Proportions of patients who achieved the target HR [77]

The bar charts illustrate the proportion of patients who reached a HR ≤ 60 bpm and the proportion of patients who reached a HR ≤ 65 bpm in the esmolol and metoprolol groups.

None of the patients developed bradycardia (defined as HR < 50 bpm) after β -blocker administration (minimum HR in the esmolol group was 53 bpm; minimum HR in the metoprolol group was 52 bpm). However, hypotension (defined as systolic BP < 100 mm Hg) was observed in 19 patients (9.3%) in the esmolol group and in 8 patients (3.8%) in the metoprolol group right after the scan (T3; $p < 0.05$). Importantly, only 5 patients (2.5%) had a systolic BP < 100 mmHg 30 minutes after the scan (T4) in the esmolol group, whereas the number of patients with hypotension remained 8 (3.8%) in the metoprolol group ($p = 0.418$). None of the patients required hospitalization or medical intervention due to hypotension and the systolic BP normalized after a short (maximum 2 hours) observation in every case. Of note, the absolute time spent in the CT unit (T2-T3) did not differ between the esmolol and metoprolol group (21.1 ± 7.5 vs. 21.8 ± 7.9 minutes; $p = 0.428$).

4.3 Heritability estimates of aortic root dimensions by CTA and TTE

This study consisted of 198 twins (118 MZ, 80 DZ; mean age for MZ 54.5 ± 9.7 and DZ 58.3 ± 8.4 years; 126 female) who prospectively underwent both CTA and TTE. Patient characteristics are provided in detail in **Table 7**. No significant differences were found between MZ and DZ twins except for age ($p=0.004$). CTA and TTE-derived diameters as well as inter-modality differences are shown in **Table 8**.

Table 7. Demographic characteristics of the study population [81]

Continuous variables are presented as mean values \pm SD, while categorical as n (%). p values represent statistical tests done between the MZ and DZ subgroups. BMI: Body Mass Index; SBP: Systolic Blood Pressure; DBP: Diastolic Blood Pressure; HT: Hypertension; DM: Diabetes Mellitus; DLP: Dyslipidaemia; MZ: monozygotic twins; DZ: dizygotic twins

	Total (n = 198)	MZ (n = 118)	DZ (n = 80)	<i>p</i>
Female (n)	126 (63.6%)	70 (59.3%)	56 (70.0%)	0.13
Age (y)	56.1 ± 9.4	54.5 ± 9.7	58.3 ± 8.4	0.004
Waist (cm)	97.1 ± 14.1	96.8 ± 14.4	97.5 ± 13.7	0.73
Height (cm)	166.4 ± 9.7	166.4 ± 10.1	166.5 ± 9.0	0.98
Weight (kg)	77.4 ± 17.3	77.5 ± 17.9	77.1 ± 16.4	0.87
BMI (kg/m ²)	27.8 ± 5.3	27.8 ± 5.0	27.9 ± 5.8	0.93
SBP (mmHg)	139.4 ± 20.4	138.4 ± 19.4	141.0 ± 21.7	0.38
DBP (mmHg)	85.7 ± 12.4	85.2 ± 12.5	86.5 ± 12.3	0.50
HT (n)	83 (41.9%)	46 (39.0%)	37 (46.3%)	0.31
DM (n)	18 (9.1%)	12 (10.2%)	6 (7.5%)	0.52
DLP (n)	83 (41.9%)	44 (37.3%)	39 (48.8%)	0.11
Current smoker (n)	29 (14.6%)	17 (14.4%)	12 (15.0%)	0.91

Table 8. Aortic root diameter measurements in millimetres (mm) as assessed by computed tomography angiography and transthoracic echocardiography

CTA: computed tomography angiography; TTE: transthoracic echocardiography; LVOT: left ventricular outflow tract

Variable (mm)	CTA				TTE				Inter-modality
	Total (n = 198)	MZ (n = 118)	DZ (n = 80)	<i>p</i>	Total (n = 186)	MZ (n = 108)	DZ (n = 78)	<i>p</i>	<i>p</i>
LVOT	23.2 ± 2.4	23.2 ± 2.5	23.3 ± 2.2	0.92	18.9 ± 2.3	18.9 ± 2.4	18.9 ± 2.2	0.99	<0.001
Annulus	23.4 ± 2.1	23.3 ± 2.2	23.5 ± 1.9	0.43	19.7 ± 2.4	19.8 ± 2.3	19.5 ± 2.5	0.52	<0.001
Sinus of Valsalva	32.8 ± 3.6	32.7 ± 3.4	32.9 ± 3.7	0.69	33.0 ± 5.1	33.5 ± 5.3	32.3 ± 4.7	0.11	0.34
Sinotubular junction	28.2 ± 3.1	27.9 ± 2.9	28.7 ± 3.4	0.07	25.5 ± 3.3	25.1 ± 3.3	26.1 ± 3.4	0.05	<0.001
Ascending aorta	30.5 ± 3.6	30.2 ± 3.4	30.9 ± 3.6	0.13	30.7 ± 3.9	30.5 ± 3.9	31.0 ± 4.0	0.41	0.12

Both CTA- and TTE-measured diameters were similar between MZ and DZ twins. In terms of inter-modality, CTA and TTE-derived parameters were significantly different regarding LVOT, annulus, and sinotubular junction (all $p<0.001$), however, the diameter of the sinus of Valsalva and ascending aorta were similar ($p=0.34$; $p=0.12$, respectively). The intra-reader reproducibility of both CTA (range: 0.98-0.99) and TTE (range: 0.96-0.99) was excellent. The inter-reader reproducibility was lower for all aortic measurements using TTE (range: 0.58-0.94) compared to CTA (range: 0.94-0.99). The intra- and inter-reader reproducibility results are summarized in **Table 9**.

Table 9. Inter-reader and intra-reader intraclass correlation coefficient results by imaging modality

Confidence intervals (CI) are shown in parenthesis. CTA: computed tomography angiography; TTE: transthoracic echocardiography; ICC: Intraclass correlation coefficients

Variable	CTA		TTE	
	Inter-reader ICC (95% CI)	Intra-reader ICC (95% CI)	Inter-reader ICC (95% CI)	Intra-reader ICC (95% CI)
LVOT	0.99 (0.97 - 0.99)	0.99 (0.97 - 0.99)	0.59 (0.35 - 0.76)	0.98 (0.97 - 0.99)
Annulus	0.94 (0.89 - 0.97)	0.99 (0.97 - 0.99)	0.58 (0.33 - 0.75)	0.96 (0.94 - 0.98)
Sinus of Valsalva	0.99 (0.98 - 0.99)	0.99 (0.99 - 1.00)	0.88 (0.79 - 0.93)	0.97 (0.94 - 0.98)
Sinotubular junction	0.95 (0.92 - 0.98)	0.98 (0.97 - 0.99)	0.77 (0.61 - 0.87)	0.96 (0.92 - 0.97)
Ascending aorta	0.99 (0.98 - 0.99)	0.99 (0.98 - 1.00)	0.94 (0.90 - 0.97)	0.99 (0.97 - 0.99)

Co-twin correlations were calculated regarding the aortic root measurements for MZ and DZ twins (**Table 10**). Higher intra-pair correlation values were observed in the MZ twins compared to DZ twins with both imaging modalities, however differences between the correlation values were higher using CTA-based measurements.

Table 10. Correlation coefficient values of MZ and DZ twins measured aortic root diameters using computed tomography and echocardiography

r_{MZ} : Co-twin Pearson correlation coefficient among MZ twins; r_{DZ} : Co-twin Pearson correlation coefficient among DZ twins; CTA: computed tomography angiography; TTE: transthoracic echocardiography; LVOT: left ventricular outflow tract

Variable	CTA		TTE	
	r_{MZ}	r_{DZ}	r_{MZ}	r_{DZ}
LVOT	0.89	0.60	0.51	0.46
Annulus	0.90	0.58	0.60	0.59
Sinus of Valsalva	0.91	0.69	0.67	0.65
Sinotubular junction	0.88	0.52	0.65	0.50
Ascending aorta	0.84	0.47	0.76	0.54

Structural equation modelling was used to decompose the total variance between the twins to genetic and environmental components. Models were adjusted for age, sex, height and diastolic blood pressure based on linear regression results. For all CTA-derived parameters, ADE models had better fit compared to ACE models based on AIC and BIC values. Even though ADE models were selected based on CTA measurements, the dominant genetic component was dropped out in all cases based on likelihood ratio tests, resulting AE models for all parameters (LVOT: A=0.67, E=0.33; annulus: A=0.76, E=0.24; sinus of Valsalva: A=0.83, E=0.17; sinotubular junction: A=0.82, E=0.18; ascending aorta: A=0.75, E=0.25). Interestingly, in case of TTE-derived measurements, ACE models showed a better fit as compared to ADE models in all cases. LVOT and ascending aorta parameters resulted in AE models while annulus, sinus of Valsalva and sinotubular junction resulted in CE models based on likelihood

ratio tests (LVOT: A=0.38, E=0.62; annulus: C=0.47, E=0.53; sinus of Valsalva: C=0.63, E=0.37; sinotubular junction: C=0.45, E=0.55; ascending aorta: A=0.67, E=0.33). Results are represented in **Figure 19** and detailed statistics are available in **Table 11 and 12**.

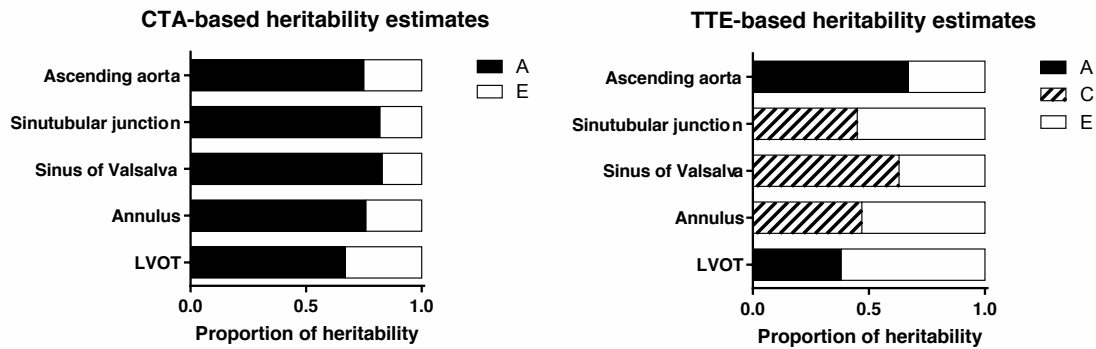


Figure 19. Heritability estimates of aortic root parameters using CTA and TTE [81]

In case of CTA-based measurements, AE models were most parsimonious, which suggests a strong genetic determination of the aortic metrics. TTE-derived measurements showed AE models for ascending aorta and LVOT and CE models for sinotubular junction, sinus of Valsalva and annulus, which suggests moderate to no genetic influence on the aortic root.

CTA: computed tomography angiography; TTE: Transthoracic echocardiography; A: additive genetic effects; C: common environmental effects; E: unique environmental effects; LVOT: left ventricular outflow tract

Table 11. Detailed results of structured equation models (ACE and ADE) for aortic root diameters measured by CTA

Bootstrapped confidence intervals are represented in parenthesis. * indicates most parsimonious full model based on AIC and BIC values.

† indicates most parsimonious submodel based on likelihood difference test. A: additive genetic effects; C: common environmental effects;

D: dominant genetic effects; E: unique environmental effects; -2LL: minus 2 log-likelihood values; AIC: Akaike information criterion;

BIC: Bayesian information criterion; df: degrees of freedom

Variable	Full model	Estimated parameters	A	C or D	E	Difference to Likelihood ratio test					Difference to Full model -2LL	Difference to Full model df	Difference to Full model p
						-2LL	Saturated model -2LL	p	AIC	BIC			
LVOT	ACE	ACE	0.68 (0.26 - 0.80)	0.00 (0.00 - 0.37)	0.32 (0.20 - 0.51)	714.83	17.80	0.01	334.83	158.24	0.00	1	1.00
		AE	0.68 (0.50 - 0.80)		0.32 (0.20 - 0.50)	714.83	17.80	0.01	332.83	162.84			
		CE		0.54 (0.35 - 0.67)	0.46 (0.33 - 0.64)	725.42	28.38	<0.001	343.42	152.25			
		E			1.00 (1.00 - 1.00)	758.46	61.43	<0.001	374.46	123.80			
	ADE*	ADE	0.00 (0.00 - 0.73)	0.68 (0.00 - 0.80)	0.32 (0.20 - 0.48)	713.35	16.32	0.01	333.35	159.72	1.48	1	0.22
		AE†	0.67 (0.50 - 0.80)		0.33 (0.21 - 0.50)	714.83	17.80	0.01	332.83	162.84			
					1.00 (1.00 - 1.00)	758.46	61.43	<0.001	374.46	123.80			
		E											
Annulus	ACE	ACE	0.76 (0.60 - 0.85)	0.00 (0.00 - 0.00)	0.24 (0.15 - 0.38)	647.55	11.20	0.08	267.55	225.52	0.00	1	1.00
		AE	0.76 (0.60 - 0.85)		0.24 (0.15 - 0.40)	647.55	11.20	0.13	265.55	230.11			
		CE		0.55 (0.34 - 0.68)	0.45 (0.32 - 0.66)	667.10	30.75	<0.001	285.10	210.57			
		E			1.00 (1.00 - 1.00)	701.58	65.23	<0.001	317.58	180.68			
	ADE*	ADE	0.00 (0.00 - 0.66)	0.76 (0.04 - 0.84)	0.24 (0.15 - 0.37)	644.37	8.01	0.24	264.37	228.71	3.19	1	0.07
		AE†	0.76 (0.60 - 0.85)		0.24 (0.14 - 0.40)	647.55	11.20	0.13	265.55	230.11			
					1.00 (1.00 - 1.00)	701.58	65.23	<0.001	317.58	180.68			
		E											
Sinus of Valsalva	ACE	ACE	0.83 (0.57 - 0.89)	0.00 (0.00 - 0.26)	0.17 (0.11 - 0.26)	870.39	9.92	0.13	490.39	-2.68	0.00	1	1.00
		AE	0.83 (0.74 - 0.89)		0.17 (0.11 - 0.26)	870.39	9.92	0.19	488.39	-7.28			
		CE		0.61 (0.46 - 0.71)	0.39 (0.29 - 0.54)	892.37	31.90	<0.001	510.37	14.70			
		E			1.00 (1.00 - 1.00)	937.36	76.90	<0.001	553.36	55.10			
	ADE*	ADE	0.67 (0.00-0.87)	0.16 (0.00 - 0.84)	0.17 (0.12 - 0.26)	870.27	9.80	0.13	490.27	-2.80	0.12	1	0.73
		AE†	0.83 (0.74 - 0.89)		0.17 (0.11 - 0.26)	870.39	9.92	0.19	488.39	-7.28			
					1.00 (1.00 - 1.00)	937.36	76.90	<0.001	553.36	55.10			
		E											
Sinotubular junction	ACE	ACE	0.82 (0.55 - 0.89)	0.00 (0.00 - 0.24)	0.18 (0.11 - 0.28)	855.52	21.43	<0.001	479.52	-6.45	0.00	1	1.00
		AE	0.82 (0.71 - 0.89)		0.18 (0.11 - 0.29)	855.52	21.43	<0.001	477.52	-11.04			
		CE		0.54 (0.36 - 0.68)	0.46 (0.32 - 0.65)	877.71	43.62	<0.001	499.71	11.15			
		E			1.00 (1.00 - 1.00)	911.79	77.70	<0.001	531.79	40.64			
	ADE*	ADE	0.47 (0.00 - 0.85)	0.36 (0.00 - 0.86)	0.17 (0.11 - 0.26)	854.86	20.77	<0.001	478.86	-7.12	0.67	1	0.41
		AE†	0.82 (0.71 - 0.89)		0.18 (0.11 - 0.29)	855.52	21.43	<0.001	477.52	-11.04			
					1.00 (1.00 - 1.00)	911.79	77.70	<0.001	531.79	40.64			
		E											
Ascending aorta	ACE	ACE	0.75 (0.23 - 0.84)	0.00 (0.00 - 0.46)	0.25 (0.15 - 0.41)	926.48	3.17	0.67	550.48	64.51	0.00	1	1.00
		AE	0.75 (0.60 - 0.85)		0.25 (0.15 - 0.40)	926.48	3.17	0.79	548.48	59.92			
		CE		0.55 (0.35 - 0.70)	0.45 (0.29 - 0.65)	939.14	15.83	0.01	561.14	72.58			
		E			1.00 (1.00 - 1.00)	974.95	51.64	<0.001	594.95	103.80			
	ADE*	ADE	0.57 (0.00 - 0.82)	0.18 (0.00 - 0.81)	0.25 (0.15 - 0.39)	926.34	3.03	0.69	550.34	64.37	0.14	1	0.71
		AE†	0.75 (0.59 - 0.85)		0.25 (0.15 - 0.41)	926.48	3.17	0.79	548.48	59.92			
					1.00 (1.00 - 1.00)	974.95	51.64	<0.001	594.95	103.80			
		E											

Table 12. Detailed results of structured equation models (ACE and ADE) for aortic root diameters as measured by TTE

Bootstrapped confidence intervals are represented in parenthesis. * indicate most parsimonious full model based on AIC and BIC values.

† indicates most parsimonious submodel based on likelihood difference test. A: additive genetic effects; C: common environmental effects; D: dominant genetic effects; E: unique environmental effects; -2LL: minus 2 log-likelihood values; AIC: Akaike information criterion; BIC: Bayesian information criterion; df: degrees of freedom

Variable	Full model	Estimated parameters	A	C or D	E	-2LL	Difference to Saturated model -2LL	Likelihood ratio test p	AIC	BIC	Difference to Full model -2LL	Difference to Full model df	Difference to Full model p
LVOT	ACE*	ACE	0.29 (0.00 - 0.52)	0.09 (0.00 - 0.52)	0.62 (0.44 - 0.90)	790.62	7.29	0.30	430.62	-27.18			
		AE†	0.38 (0.09 - 0.56)		0.62 (0.44 - 0.91)	790.67	7.34	0.39	428.67	-31.66	0.06	1	0.81
		CE		0.33 (0.07 - 0.52)	0.67 (0.48 - 0.92)	791.16	7.83	0.35	429.16	-31.18	0.54	1	0.46
	ADE	E			1.00 (1.00 - 1.00)	801.79	18.46	0.02	437.79	-25.09	11.18	2	<0.001
		ADE	0.38 (0.00 - 0.53)	0.00 (0.00 - 0.50)	0.62 (0.44 - 0.89)	790.67	7.34	0.29	430.67	-27.12			
		AE	0.38 (0.09 - 0.56)		0.62 (0.43 - 0.91)	790.67	7.34	0.39	428.67	-31.66	0.00	1	1.00
Annulus	ACE*	E			1.00 (1.00 - 1.00)	801.79	18.46	0.02	437.79	-25.09	11.12	2	<0.001
		ACE	0.14 (0.00 - 0.64)	0.36 (0.00 - 0.57)	0.50 (0.31 - 0.71)	787.52	3.87	0.69	427.52	-30.27			
		AE	0.53 (0.31 - 0.69)		0.47 (0.31 - 0.69)	789.05	5.40	0.61	427.05	-33.29	1.53	1	0.22
	ADE	CE†		0.47 (0.29 - 0.62)	0.53 (0.38 - 0.74)	787.74	4.09	0.77	425.74	-34.60	0.22	1	0.64
		E			1.00 (1.00 - 1.00)	810.96	27.32	<0.001	446.96	-15.92	23.44	2	<0.001
		ADE	0.53 (0.00 - 0.69)	0.00 (0.00 - 0.50)	0.47 (0.30 - 0.72)	789.05	5.40	0.49	429.05	-28.74			
Sinus of Valsalva	ACE*	AE	0.64 (0.41 - 0.84)		0.36 (0.16 - 0.59)	1063.8	16.37	0.02	705.83	252.50	5.33	1	0.02
		CE†		0.63 (0.44 - 0.78)	0.37 (0.22 - 0.56)	1058.5	11.04	0.14	700.50	247.17	0.00	1	1.00
		E			1.00 (1.00 - 1.00)	1104.6	57.09	<0.001	744.55	288.68	46.05	2	<0.001
	ADE	ADE	0.64 (0.41 - 0.83)	0.00 (0.00 - 0.00)	0.36 (0.16 - 0.58)	1063.8	16.37	0.01	707.83	257.03			
		AE	0.64 (0.41 - 0.83)		0.36 (0.16 - 0.58)	1063.8	16.37	0.02	705.83	252.50	0.00	1	1.00
		E			1.00 (1.00 - 1.00)	1104.6	57.09	<0.001	744.55	288.68	40.72	2	<0.001
Sinotubular junction	ACE*	ACE	0.26 (0.00 - 0.75)	0.25 (0.00 - 0.53)	0.49 (0.22 - 0.70)	808.23	8.28	0.22	492.23	110.06			
		AE	0.53 (0.32 - 0.77)		0.47 (0.23 - 0.69)	808.95	8.99	0.25	490.95	106.35	0.72	1	0.40
		CE†		0.45 (0.26 - 0.59)	0.55 (0.41 - 0.74)	808.88	8.92	0.26	490.88	106.28	0.64	1	0.42
	ADE	E			1.00 (1.00 - 1.00)	827.34	27.39	<0.001	507.34	120.33	19.11	2	<0.001
		ADE	0.53 (0.00 - 0.72)	0.00 (0.00 - 0.64)	0.47 (0.21 - 0.69)	808.95	8.99	0.17	492.95	110.77			
		AE	0.53 (0.31 - 0.77)		0.47 (0.22 - 0.69)	808.95	8.99	0.25	490.95	106.35	0.00	1	1.00
Ascending aorta	ACE*	E			1.00 (1.00 - 1.00)	827.34	27.39	<0.001	507.34	120.33	18.39	2	<0.001
		ACE	0.48 (0.00 - 0.79)	0.18 (0.00 - 0.56)	0.34 (0.19 - 0.56)	898.31	4.65	0.59	558.31	135.25			
		AE†	0.67 (0.45 - 0.82)		0.33 (0.18 - 0.55)	898.75	5.09	0.65	556.75	131.20	0.44	1	0.51
	ADE	CE		0.55 (0.37 - 0.68)	0.45 (0.32 - 0.63)	901.68	8.02	0.33	559.68	134.13	3.37	1	0.07
		E			1.00 (1.00 - 1.00)	933.64	39.98	<0.001	589.64	161.60	35.33	2	<0.001
		ADE	0.67 (0.00 - 0.80)	0.00 (0.00 - 0.65)	0.33 (0.18 - 0.54)	898.75	5.09	0.53	558.75	135.68			
ADE	AE	0.67 (0.45 - 0.81)		0.33 (0.19 - 0.54)	898.75	5.09	0.65	556.75	131.20	0.00	1	1.00	
	E			1.00 (1.00 - 1.00)	933.64	39.98	<0.001	589.64	161.60	34.89	2	<0.001	

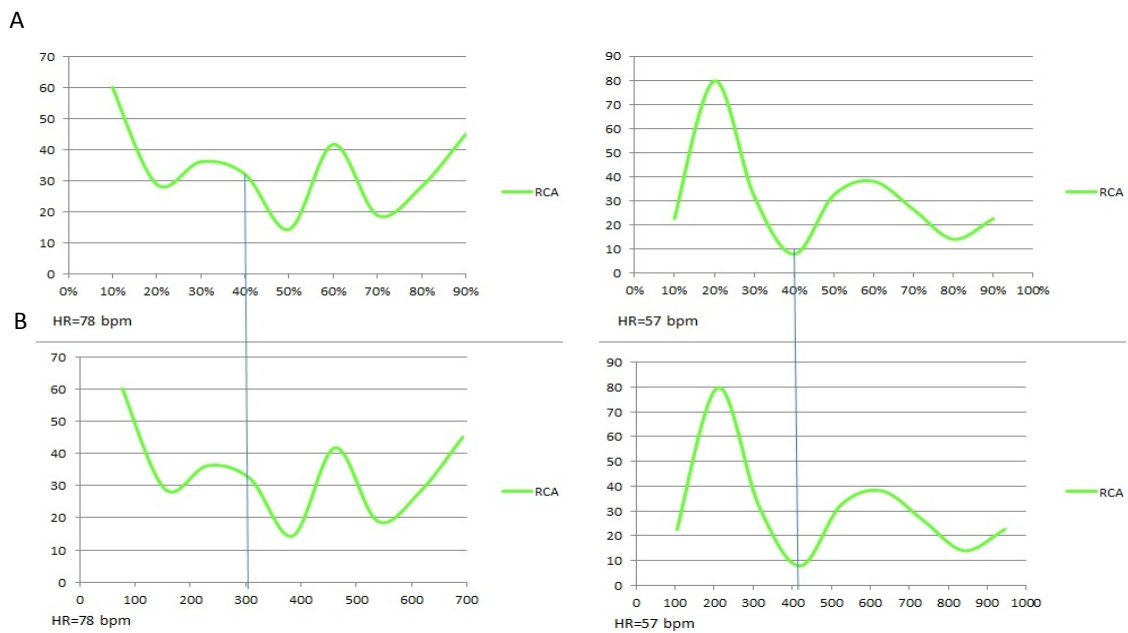
5. DISCUSSION

5.1 Systolic image reconstruction by using absolute delay

We found that coronary artery velocity during late systole is independent of HR and between 260-340 ms mean velocities were significantly lower. The relatively fixed length of the systole versus diastole is a well-understood phenomenon. At higher HRs, the diastasis period shortens, and above HR of 96 bpm it eventually disappears [31, 88, 89]. Thus, cardiac CT phase reconstructions at end-systole are often considered. Several previous studies investigated image acquisitions performed during this period [4, 37, 90-92]. One study sought to assess the optimal systolic and diastolic phase reconstruction during coronary CTA [4]. Motion of the coronary arteries was scored on a 1-5 motion scale (1: no motion artifacts; 5: severe motion artifacts), in 5% steps throughout the R-R interval. In patients with HR<70 bpm, significantly lower scores were found during diastole vs. systole, while in patients with HR>80 bpm, systole provided significantly lower motion scores. The least coronary motion during diastole was found at 75% reconstruction window and during systole at 30% and 35% reconstruction windows. Another study evaluated the robustness of the end-systolic temporal windows in patients with HR>65 bpm [90]. In contrast with the previous study motion of the coronary arteries was evaluated during a predefined temporal window of 200-400 ms. Results suggest, that a 100 ms long end-systolic temporal window is able to provide acceptable image quality at any heart rate. A prior investigation [31] directly compared the image quality and artifacts of the aortic and mitral valves using relative and absolute delay reconstructions. Their results indicate that the absolute delay image reconstruction provides superior image quality with less motion artifacts. These differences are due to HR variability, as in patients with higher HR the diastole shortens which leads to the non-proportional decrease of the R-R interval [35]. For example, in a patient with HR of 78 bpm (R-R cycle length of 770 ms), a 40 % relative R-R phase reconstruction corresponds to 308 ms (i.e. mid systole), whereas at a heart rate of 57 bpm (R-R cycle length of 1,050 ms), a reconstruction interval, placed at 40 % displaces to a 420 ms absolute delay (i.e. end-systole) (**Table 13 and Figure 20**). Therefore when using traditional relative phase percentage reconstructions the specified period of the cardiac cycle is highly variable at differing HRs.

Table 13. Reconstruction times at 10 % phase increment for HR = 78 and 57 bpm [75]

HR = 78 bpm Phases (%)	Time (ms)	Velocity (mm/s)	HR = 57 bpm Phases (%)	Time (ms)	Velocity (mm/s)
10	77	60.2	10	105	22.6
20	154	28.9	20	210	79.8
30	231	36.2	30	315	32.0
40	308	32.2	40	420	7.9
50	385	14.4	50	525	32.5
60	462	41.8	60	630	38.1
70	539	18.9	70	735	26.3
80	616	28.2	80	840	14.0
90	693	45.1	90	945	22.6

**Figure 20.** Relative vs. absolute reconstruction interval at HR of 78 and 57 bpm [75]

Velocity maps of two different patients' RCAs using A: relative delay (% of the R-R interval, x-axis), and B: absolute delay (ms of the R-R interval, x-axis) demonstrate differences in minimal systolic velocities. Vertical line is placed at 40 % of the R-R cycle, which at HR of 78 bpm corresponds to an absolute delay of 308 ms and at HR of 57 bpm to an absolute delay of 420 ms. Note that despite highly disparate HR, the minimal velocity time point lies similarly close to 400 ms after the R-wave.

In our study the image reconstructions performed using an absolute delay resulted in selected phases with good or excellent image quality in all patients, as clinically deemed and reported. Thus all selected coronary artery landmarks could be visualized and their location precisely analyzed, albeit at slightly differing time points. Accordingly, we calculated the optimal velocities of the selected coronary arteries and examined the motions' HR dependency. We found no significant correlation between the HR and coronary artery motion velocities, except for the AM1 branch.

The selected absolute delay interval in our study (200-420 ms) corresponds to the time-interval of the ventricular systole and extends between the peak of the R-wave and the T-wave or the descending T-wave of the electrocardiogram. Physiologically, ventricular systole is divided into two periods: the isovolumic contraction phase and the ejection phase. The ejection phase consists of an early phase when the maximum ejection occurs and a latter phase with reduced or absent ejection [35]. The reduced phase is immediately followed by the proto-diastole and the isovolumic relaxation. Physiological investigations revealed an inert systolic phase with a constant low motion at the end of systole and early diastole, thus providing a basis for late-systolic/early diastolic cardiac CT acquisitions [32].

A previous study sought to assess the durations of the left ventricular systolic phases, including the isovolumic contraction time (ICT), the pre-ejection period (PEP) and the left ventricular ejection time (LVET) [93]. According to their measurements, the mean ICT was 70 ± 9.5 ms with a range of 51-90 ms, the mean PEP was 100 ± 13 ms with a range of 78-130 ms and the mean LVET was 281 ± 21 ms, ranging from 230 to 334 ms. In our study we found that the optimal time points with lowest coronary motion ranged from an average phase start time of 273 ms in the origin of the LM to 329 ms in the AM branch (**Table 2**). These findings are congruent with our findings that the mean coronary artery motion velocities were significantly lower in the mid period of the selected temporal window, between 280 and 340 ms (**Figure 16**). Thus we found that the lowest coronary motion occurs during the LVET, in its second half during reduced ejection through the following proto-diastole, and confirms the previous works reporting the existence of an inert constant low motion end-systolic early diastolic temporal window.

To our knowledge, no other previous studies have investigated the image quality during the end-systolic temporal window by using absolute delay image reconstruction based on the coronary artery motion in patients with different HRs.

We believe our findings have three applications in the current era of cardiac CT. First, as prior work has established, systolic targets are highly useful in the setting of tachycardia and arrhythmia, in order to salvage diagnostic coronary CTA [4]. Second, as described in the multimodality imaging guideline for aortic valve intervention, evaluation can be improved by systolic absolute-delay reconstructions, of particular importance given the now well-established role of cardiac CTA for TAVI planning [94]. Third, the field of myocardial stress perfusion CT is emerging, and image acquisitions are performed during the administration of pharmacologic vasodilator stress agents; these agents raise HRs, often shortening or eliminating diastolic windows for acquisition. Because acute beta-blockade has been shown to decrease the efficacy of pharmacologic stress, the ability to image in systole may be a key element to the performance of stress perfusion CT, which is technically challenging and depends upon concomitant coronary artery imaging [95, 96].

5.2 The use of esmolol before coronary CTA

In this randomized, single-center clinical trial we compared IV esmolol vs. IV metoprolol for HR control in patients who underwent coronary CTA because of suspected CAD. We showed that esmolol with a stepwise bolus administration protocol is at least as efficacious as the standard of care metoprolol to achieve the optimal HR (<65 bpm) during coronary CTA. Furthermore, we have demonstrated that IV esmolol allows a safe HR control for coronary CTA examination even if it is administered in relatively high doses with a dosage scheme independent of body weight.

Esmolol is an ultrashort-acting IV β -blocker. The rapid onset and offset of effects of esmolol make this IV drug a potential alternative of the standard of care metoprolol in the daily routine coronary CTA service. Especially, coronary CTA services with no access to cardiology or intensive care background might benefit most of this ultrashort-acting medication. The recommended administration protocol of IV esmolol with infusion pump is relatively complex and precluded its widespread use in the diagnostic facilities. Different dosage schedules have been developed depending on clinical setting and diagnosis. Generally, a loading dose of <500 $\mu\text{g}/\text{kg}/\text{min}$ over 1 minute is administered followed by a continuous infusion of 25–300 $\mu\text{g}/\text{kg}/\text{min}$ [82]. We showed that esmolol is safe and efficacious if administered in boluses without the subsequent continuous infusion. The “bolus only” administration protocol of esmolol would make this IV β -blocker a real life alternative of IV metoprolol. In this clinical trial we used a body weight-independent administration protocol with stepwise increments in dose in every 3 minutes. Importantly, the timing of the administration of the IV esmolol boli was similar to the metoprolol administration protocol; therefore, it did not slow down our routine clinical cardiac CT workflow. Our choice of 100-mg IV esmolol for the initial bolus is based on a previous observational study that showed that the dose of 2 mg/kg (for a 70-kg patient this equals 140-mg esmolol) is safe to administer before the coronary CTA examination [97]. If 100-mg dose proved to be ineffective, and the patients' HR did not reach the predefined ≤ 65 bpm in 3 minutes, we have increased the bolus to 200-mg IV esmolol. Finally, if the HR did not change after an additional 3-minute period (testing during a Valsalva maneuver as well), we administered the third, once again 200-mg, bolus of IV esmolol. We have not added further boluses; thus, the maximum administered IV esmolol was 500 mg during an approximately 6- to 7-

minutes time period. Of note, only about one-third of patients have received the full dose of esmolol and two-thirds of patients have reached the target HR with ≤ 300 -mg esmolol dose. We have stopped the patient enrollment as early as the interim analysis indicated that esmolol is clearly non-inferior to metoprolol; in fact, it showed superiority characteristics as the responder proportion in the esmolol group was 89% vs. the metoprolol group's 78%.

A previous study [97] demonstrated the safety and efficacy of IV esmolol in 391 patients. In this prospective study, HR was reduced from 80 ± 11 bpm to 63 ± 7 bpm and HR < 65 bpm was achieved in 65% of the patients. Four of the 391 patients (1%) have experienced a final HR of < 50 bpm; however, all 4 remained asymptomatic and the bradycardia resolved in minutes without any intervention with atropine or temporary pacing. Moreover, this study reported a 0.5% incidence of transient hypotension (systolic BP < 100 mm Hg). In our clinical trial, we have reached a higher responder proportion (89.2%) probably because of a more aggressive dosing scheme. Importantly, none of the 204 patients who received esmolol had severe bradycardia (minimum HR was 53 bpm). On the other hand, transient hypotension (systolic BP < 100 mm Hg) was observed in 9.3% of the patients immediately after the scan in the esmolol group, which was significantly higher compared to the metoprolol groups' 3.8%. Importantly, 30 minutes after the scan this decreased to 2.5% in the esmolol group, whereas in the metoprolol group the percentage of patients with hypotension did not change (3.8%). None of the patients had clinically significant adverse event. Thus, the stepwise bolus administration of esmolol is safe and it is well tolerated among patients with normal left ventricular function scheduled to undergo coronary CTA examination. Furthermore, our data show that IV esmolol is at least as efficacious as IV metoprolol to reach optimal HR during coronary CTA.

Many centers are reluctant to administer IV medication for HR control during coronary CTA owing to the fear from potential side effects. Another study [98] reported minor complications (transient hypotension) related to IV metoprolol administration only in 1.47% and major complications (not resolving with observation of analgesia) in 0.44% of patients who underwent coronary CTA. These results demonstrate that IV metoprolol is a safe drug to use for this purpose in patients with normal left ventricular function although the study was underpowered to assess for rare major complications.

Esmolol is metabolized via rapid hydrolysis by red blood cell esterases, independent of the hepatic and renal function [99]. It is routinely administered during perioperative intensive care and before laryngoscopy and tracheal intubation procedures to prevent hypertension and tachycardia [100, 101]. In this clinical trial, we have excluded patients with contraindications to β -blockers such as asthma. However, it has been demonstrated previously that esmolol is safe in bronchospastic diseases [102].

5.3 Impact of the imaging method on heritability of the aortic root

The purpose of our study was to investigate the influence of the imaging method on the heritability estimates of the aortic root dimensions. The main finding of our study is that the CTA-derived measurements suggest a stronger heritability of the aortic root configuration. TTE-derived measurements showed moderate to no genetic influence. CTA- and TTE-measured diameters were similar between MZ and DZ twins, however TTE significantly underestimated the diameters of LVOT, annulus and sinotubular junction as compared to CTA (**Table 8**).

Intra-reader reproducibility of TTE was excellent similarly to CTA, however inter-reader reproducibility of TTE was substantially lower than CTA in case of all parameters (**Table 9**).

In line with our expectations we observed stronger correlations in the MZ twins compared to DZ twins, independent of the imaging technique (**Table 10**). However, differences between MZ and DZ correlations were substantially higher when using CTA-derived measurements. These differences in correlation values might be the consequence of the inherent properties (e.g. reproducibility, accuracy) of the two imaging modalities. While TTE provides reliable functional information, CTA gives more precise anatomical evaluation. Previous studies have demonstrated that TTE-derived annulus diameters are substantially smaller compared to CTA-based measurements [69, 103]. Due to the complex shape of the annulus its diameter might vary according to the location where it was measured. Therefore underestimation might be attributable to the 2D nature of TTE, which limits precise measurement.

Measurement inconsistencies between the two imaging methods can result in differences in heritability components. A substudy of the Strong Heart Study sought to assess the heredity of aortic root diameter in family members using TTE. The heritability of the aortic root was 0.44, which indicates that a major proportion of phenotypic variance is due to environmental factors [63]. Another study that investigated the heritability of the aortic root diameter showed 0.49 heritability estimates [67].

Our TTE-based heritability estimates also confirm these findings, showing lower genetic determination of the aortic root compared to CTA. Specifically, LVOT and ascending aorta resulted in AE models, while the annulus, sinus of Valsalva and

sinotubular junction resulted in CE models, indicating the superiority of environmental factors over additive genetic factors (**Figure 19, Table 12**). Technical limitations of TTE such as suboptimal echo window, chest and body configuration of the patient contribute to the accumulation of potential measurement errors, which might appear as part of the unique environmental effects.

In case of CTA AE models showed that aortic root diameters are mostly determined by the additive effect of genes (**Figure 19, Table 11**). The superior reproducibility and precise measurement capability of CTA resulted in higher heritability estimates of aortic components. These results suggest that the extent of heritability estimates strongly depends on the imaging method.

It is recognised that genetics play an important role in the development of aortic pathology. In general, two approaches exist for the identification of genes susceptible for the trait or disorder. Candidate gene studies aim to assess the association between pre-specified genes of interest and phenotypic variance or disorder. In contrast, genome-wide association studies (GWAS) scan the entire genome and provide information of genetic variations. Previous studies demonstrated that thoracic aortic aneurysms are associated with multiple genetic mutations. TGFBR1 (transforming growth factor-beta receptor type 1) and TGFRB2 mutations are frequently identified in aortic aneurysms [104, 105] and are responsible for pathological aortic tissue degeneration, so called cystic medial necrosis [106]. A combined GWAS and candidate gene study investigated 11 families with aortic aneurysms and discovered a novel mutation in gene TGFBR3, which is also significantly associated with thoracic and abdominal aneurysm as well as mitral valve disease [107]. Aortic aneurysms showed strong familial accumulation, therefore authors recommended a close-follow up of family members and yearly echocardiographic imaging of the aortic root with at least one baseline imaging of the whole aorta including side branches in patients carrying this mutation.

CTA plays a key role for diagnosing patients at potential risk for aortic aneurysms. Despite the drawback of the radiation exposure and the administration of IV contrast agent, CTA provides precise measurement of the complex configuration of the aorta and side branches. Moreover, it is able to assess calcifications and thrombi, thus providing better risk stratification of patients undergoing surgical procedures.

5.4 Limitations

There are some limitations regarding the listed studies that have to be considered.

The optimal systolic phase investigations has a small cohort of 21 patients, however it is sufficient number to give 1488 landmark points for velocity evaluation. This study was also a single center and a single vendor study. We used a second-generation dual source scanner, which gave temporal resolution of 75 ms, which is relatively low as compared to commonly available single-source scanners; since our data was acquired, native temporal resolutions have been decreased to 66 ms with more modern scanners. Motion could also be confounded by respiratory motion artifact, which is very difficult to subtract from the final image. Lastly, our vendor's definition of a phase was the "phase start"; whereas other vendors may define a phase reconstruction by the "phase center" and this careful distinction is important if generalizing our findings to other systems.

The esmolol vs. metoprolol study was a single-center study; therefore, the efficacy and safety of the described esmolol bolus protocol has to be evaluated in a multicenter randomized controlled trial. As the administration protocols and the injected volumes were different for the IV metoprolol and IV esmolol groups, it was not feasible to blind the physicians to the drug they were administering. The combined use of oral and IV β -blocker protocols for HR control might limit the generalizability of our results for IV-only protocols. Owing to the oral metoprolol pretreatment, our findings do not demonstrate that esmolol IV alone vs. metoprolol IV is as or more effective for HR control. However, it is important to note that the combined use of oral and IV β -blockers is a widely used and effective strategy for HR lowering before coronary CTA [6, 108]. In this scenario, esmolol is at least as efficacious as IV metoprolol. The response rate to oral metoprolol was relatively low in our study (162 of 574 [28%]), which might have been higher with the use of a more aggressive administration regime (e.g. 100-mg oral metoprolol if HR >65 bpm) [82]. Furthermore, we did not test smaller doses of esmolol (e.g. 50–100 mg), which might be equally efficacious.

Regarding the heritability estimates of the aortic root the sample size of our population was moderate compared to population-based twin registries, nonetheless the multimodality nature of our study provides more robust measurements than earlier investigations. Second, CTA and TTE measurements were not performed exactly in the same time of the cardiac cycle (mid-diastole vs. mid-systole to end-diastole,

respectively). However, in a previous study no significant differences were found in the size of the annulus during the cardiac cycle [60]. Finally, due to the length of the TTE protocol, only one regular and one zoomed parasternal long-axis loop was acquired consisting of 3 cardiac cycles each. Optimal measurements were selected on an offline basis, which resulted in fair intra- and inter-reader reproducibility.

5.5 Future perspectives

Impaired image quality is frequently attributable to motion artifacts, which lead to higher incidence of non-diagnostic coronary segments. Image acquisition during systole is of great importance in patients with higher and/or variable HR, when the length of diastole shortens.

In the past years, CTA has emerged as a non-invasive imaging technique for left atrial and pulmonary vein image acquisition in patients referred for radio-frequency catheter ablation (RFCA) [109]. The 3D nature of CTA allows for precise visualization of the complex shape of the left atrium and pulmonary veins, besides it enables to obtain CAD, which was previously shown to have higher prevalence in patients with atrial fibrillation [110, 111]. However, patients undergoing CTA before RFCA frequently show up with cardiac arrhythmia, which hampers the evaluation of the coronary arteries. By refining the systolic temporal window diagnostic image quality can be reached also in this patient population, which eventually aids the diagnosis of CAD. Moreover, in the era of TAVI procedures systolic image acquisition is increasingly important. Acquisition of the aortic root and the heart by CTA prior to TAVI is performed during systole, due to the fact that aortic annulus area and mean diameter are larger during systole [112, 113]. When performing TAVI calcifications are displaced/crushed by the prosthesis with a risk of potential coronary occlusion. A predefined systolic temporal window where the coronary arteries move the least might be very helpful to achieve precise measurement, thus avoiding future complications. Moreover, CTA is able to provide valuable information regarding the amount and distribution of calcification in the aortic root and peripheral vasculature. Reproducibility is also essential when measuring geometry of anatomical complex structures. A previous study showed that the use of automated post-processing imaging software for annular measurement before TAVI was better in predicting the occurrence of post-procedural aortic regurgitation compared with the manual measurements [114]. In our heritability study we also demonstrated that the use of semi-automated algorithm provides reliable intra and inter-reader measurements of the complex aortic root. In the future more feasibility studies regarding the use of semi/fully automated software algorithms prior to TAVI as a part of the clinical routine are expected.

Furthermore, recently several investigations focused on the detection of coronary microvascular dysfunction. The spatial resolution of current CT scanners ($\approx 400 \mu\text{m}$) limits the precise detection of microvascular disease, however future technical advances in stress induced CT myocardial perfusion might serve as a non-invasive imaging method for detecting microvascular disease [115]. Adenosine stress-rest cardiac CT is able to identify myocardial perfusion defects and as such is capable of reducing the number of false positive CTA findings [116, 117]. However, the use of adenosine entails the increase of HR, thus reducing the image quality. The end-systolic period might allow for better image quality therefore in the future the number of investigations regarding systolic image acquisitions is expected to increase.

Administration of HR lowering medications prior to CTA aids to improve image quality. To date metoprolol is the most frequently used β -blocker in patients with $\text{HR} > 65$ bpm. However, there are several conditions when the use of metoprolol is contraindicated. Our study demonstrated that the use of esmolol prior to CTA examination is simple, effective and safe. Therefore if contraindications are present esmolol is an alternative method to achieve the desirable HR and image quality. It is important to note that esmolol is more expensive than IV metoprolol. However, the effective and short duration of HR control achievable with esmolol might result in wider usage of this IV β -blocker in cardiac CT labors, which would increase the percentage of patients scanned with optimal HR and improve the diagnostic performance of CTA. A larger multicenter trial is warranted to adequately explore the cost-effectiveness of esmolol use in the coronary CTA laboratories.

Imaging with CTA revealed a greater genetic influence compared to TTE as it provides more reliable measurements of the complex aortic root. Therefore, the choice of imaging technique is crucial in heritability studies. Moreover, our study demonstrated that image acquisition by CTA is indispensable when performing structural heart disease interventions. Recently, the usefulness of CTA was shown in sizing of transcatheter caval valve implantation (CAVI) [118]. Based on 3D CTA images 3D printing of right atrium-inferior vena cava (RA-IVC) topography was performed that aided the transcatheter valve selection (**Figure 21**). Therefore in the future CTA is expected to play a key role in 3D printing and planning of complex procedures.

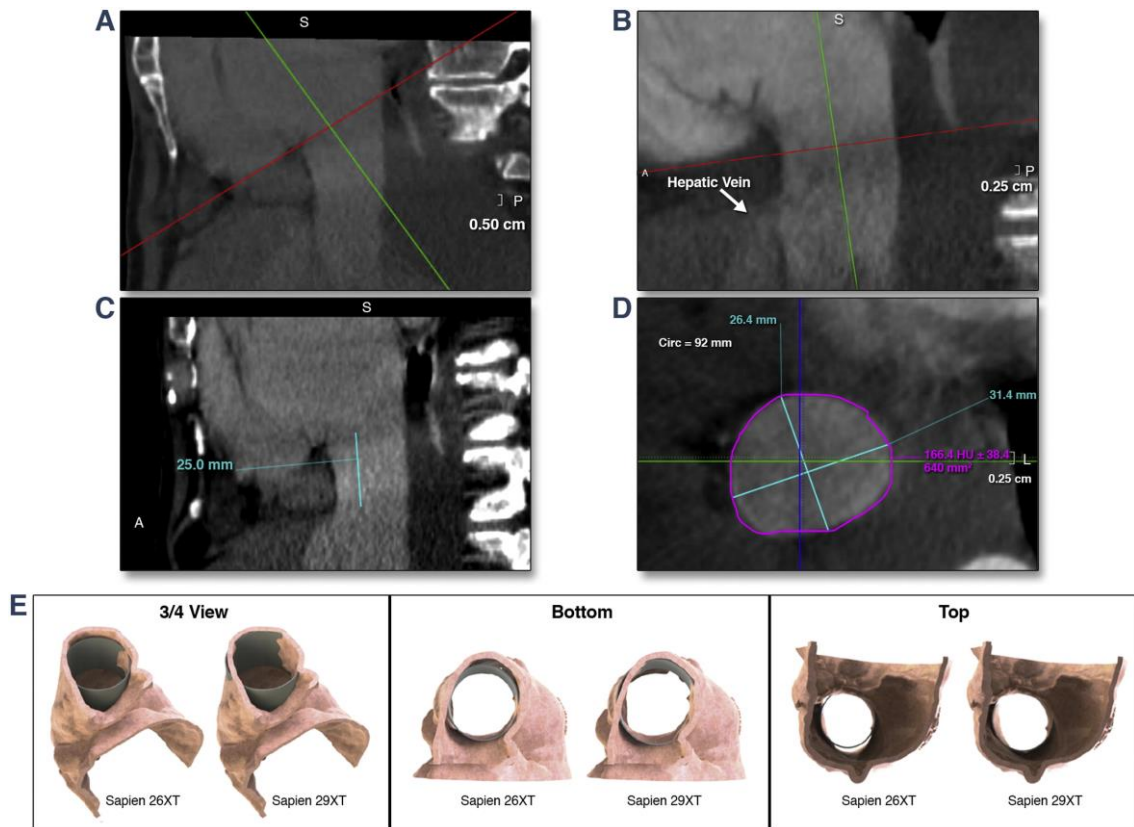


Figure 21. CTA guided 3D printing for selection of the appropriate size of SAPIEN XT Valve for caval valve implantation [118]

A: visualization of right atrium-inferior vena cava (RA-IVC) junction plane; B: the first hepatic vein; C: height measured between the two structures aids optimal valve positioning without the obstruction of the hepatic vein; D: sequential measurements in horizontal planes 1 cm below the RA-IVC junction and 1 cm above the first identified hepatic vein for valve sizing; E: 3D printed models of the RA-IVC junction with SAPIEN 26XT and 29XT (Edwards Lifesciences Corp., Irvine, California) valve mockups inserted for fit testing; When using SAPIEN 26XT valve a gap occurred between the IVC lining and the valve frame, which raised concerns about the development of perivalvular leak, hence the SAPIEN 29XT valve was chosen.

6. CONCLUSIONS

CTA is a technically demanding procedure, and motion artifacts present the chief challenge unique to ECG-gated coronary CTA. Diagnostic image quality can be achieved by synchronizing the acquisition window to the phase of the cardiac cycle with minimal coronary arterial motion. Coronary CTA image acquisitions are typically performed in the most quiescent period of the cardiac cycle, which at low and stable HR is during mid-diastole. However, in patients with higher HR, the end-systolic and early-diastolic reconstructions are more favorable. In our study we found that during an absolute delay of 200-420 ms after the R-wave, the ideal reconstruction interval varies significantly among coronary artery segments. Decreased coronary artery velocities occur between 280 to 340 ms of the cardiac cycle. Therefore a narrow range of systolic intervals, rather than a single phase should be acquired.

Coronary CTA is an established tool to rule out CAD. Diagnostic accuracy of coronary CTA is highly dependent on patients' HR. Despite widespread use of β -blockers before coronary CTA, only few studies have compared various agents used to achieve adequate HR control. In our study we sought to assess whether the ultrashort-acting β -blocker IV esmolol is at least as efficacious as the standard of care IV metoprolol for HR control during coronary CTA. Our results suggest that IV esmolol with a stepwise bolus administration protocol is at least as efficacious as the standard of care IV metoprolol for HR control in patients who undergo coronary CTA.

Heritability plays an important role in the configuration of the aortic root. Previous heritability studies of the aortic root used TTE for the assessment of aortic root dimensions and showed weak to moderate heritability. CTA might enable more accurate measurements and better estimation of heritability. In our study we showed that CTA-derived metrics resulted in stronger heritability of the aortic root, as compared to TTE-derived measurements, which showed moderate to no genetic influence. These results suggest that the imaging method has a considerable impact on the heritability estimates and metrics of the aortic root.

7. SUMMARY

In the past decade Computed Tomography Angiography (CTA) has emerged an essential diagnostic imaging modality for the evaluation of the coronary artery tree and the aortic root. Improved temporal and spatial resolution of current CT scanners allow for accurate detection of coronary atherosclerosis, while the 3-dimensional nature of CTA provides accurate and reproducible measurements of complex anatomical structures. However, precise evaluation of the images requires the optimization of image quality. Adequate timing of image acquisition and suitable use of premedication enable to achieve diagnostic image quality.

We defined the optimal systolic reconstruction interval by using absolute delays. We found that coronary artery velocity during late systole is independent of heart rate (HR) and in the mid period of the selected systolic time-interval mean coronary artery velocities were significantly lower.

We also demonstrated that ultra-short time intravenous (IV) esmolol prior to CTA is at least as efficacious, as metoprolol to achieve the optimal HR (<65 bpm). Furthermore, we have shown that IV esmolol allows for safe HR control even if it is administered in relatively high doses.

We showed that inherent properties of CTA and the use of semi-automated post-processing software allow for more accurate and reproducible measurement of aortic root dimensions compared with transthoracic echocardiography (TTE). Inaccurate measurements artificially inflate the magnitude of the environmental component in the heritability estimates of aortic root. In our twin study TTE-based measurements showed moderate to no genetic influence, while CTA-based measurements suggested that aortic root dimensions are predominantly determined by genetic factors. Therefore, the choice of imaging method has a substantial impact on heritability estimates.

Our results emphasize that optimal image quality during cardiac CTA allows for the diagnosis of coronary artery disease as well as precise and reproducible measurements of complex anatomical structures, which are utmost importance in the era of structural heart disease interventions.

8. ÖSSZEFOGLALÁS

Az elmúlt évtizedben a komputer tomográfia angiográfiának (CTA) egyre nagyobb szerepe van a koszorúerek és az aortagyök vizsgálatában. A CTA térbeli és időbeli felbontóképessége lehetővé teszi a koszorúér-betegség ábrázolását, 3 dimenziós sajátossága pontos és reprodukálható méréseket biztosít a bonyolult anatómiájú struktúrák esetében. A felvételek pontos értékelése jelentős mértékben függ a képminőségtől. A képrekonstrukció pontos időzítése, valamint a betegek megfelelő premedikációja lehetővé teszi a diagnosztikus képminőség elérését.

Munkám során megállapítottam a systolében végzett képrekonstrukció optimális fázisát. Eredményeink alapján a koszorúerek mozgási sebessége a systole késői szakasza alatt a szívfrekvenciától független, valamint a vizsgált időintervallum középső szakaszában szignifikánsan alacsonyabb, ezért a CTA vizsgálat során a systolében végzett képrekonstrukció a systole ezen szakaszában javasolt.

Munkám további részében bizonyítottam, hogy a CTA vizsgálat előtti célszívfrekvencia (<65/perc) elérésében az ultra-rövid hatású intravénás esomolol legalább annyira hatásos mint a metoprolol, valamint az esmolol akár magasabb dózisának alkalmazása is biztonságos szívfrekvenciát eredményez.

Továbbá megállapítottam, hogy a CTA sajátosságai valamint a fél-automata algoritmus használata az aortagyök átmérőinek pontosabb és reprodukálhatóbb méréseit teszi lehetővé a transztorakális echocardiográfiához (TTE) képest. A mérési pontatlanság az öröklődési vizsgálatok során "arteficiálisan" növelheti a környezeti hatások mértékét. Az általunk végzett ikervizsgálatban a TTE-vel mért átmérők mérsékelt öröklődést vagy annak teljes hiányát mutatták, míg a CTA-val végzett mérések alapján az aortagyök átmérőit leginkább a genetikai tényezők határozták meg. Ezek alapján arra következtetünk, hogy a kapott öröklődési értékek jelentős mértékben függenek a választott képalkotó módszertől.

A CTA vizsgálat során az optimális képminőség lehetővé teszi a koszorúér-betegség diagnosztizálását, valamint pontos és reprodukálható méréseket biztosít, mely a strukturális szívbetegségek intervenciójának elengedhetetlen feltétele.

9. BIBLIOGRAPHY

1. Achenbach S, Delgado V, Hausleiter J, Schoenhagen P, Min JK, Leipsic JA. (2012) SCCT expert consensus document on computed tomography imaging before transcatheter aortic valve implantation (TAVI)/transcatheter aortic valve replacement (TAVR). *J Cardiovasc Comput Tomogr*, 6: 366-380.
2. Bley TA, Ghanem NA, Foell D, Uhl M, Geibel A, Bode C, Langer M. (2005) Computed tomography coronary angiography with 370-millisecond gantry rotation time: evaluation of the best image reconstruction interval. *J Comput Assist Tomogr*, 29: 1-5.
3. Leschka S, Husmann L, Desbiolles LM, Gaemperli O, Schepis T, Koepfli P, Boehm T, Marincek B, Kaufmann PA, Alkadhi H. (2006) Optimal image reconstruction intervals for non-invasive coronary angiography with 64-slice CT. *Eur Radiol*, 16: 1964-1972.
4. Seifarth H, Wienbeck S, Pusken M, Juergens KU, Maintz D, Vahlhaus C, Heindel W, Fischbach R. (2007) Optimal systolic and diastolic reconstruction windows for coronary CT angiography using dual-source CT. *AJR Am J Roentgenol*, 189: 1317-1323.
5. Weustink AC, Mollet NR, Pugliese F, Meijboom WB, Nieman K, Heijnenbroek-Kal MH, Flohr TG, Neefjes LA, Cademartiri F, de Feyter PJ, Krestin GP. (2008) Optimal electrocardiographic pulsing windows and heart rate: effect on image quality and radiation exposure at dual-source coronary CT angiography. *Radiology*, 248: 792-798.
6. Abbara S, Arbab-Zadeh A, Callister TQ, Desai MY, Mamuya W, Thomson L, Weigold WG. (2009) SCCT guidelines for performance of coronary computed tomographic angiography: a report of the Society of Cardiovascular Computed Tomography Guidelines Committee. *J Cardiovasc Comput Tomogr*, 3: 190-204.
7. Mahabadi AA, Achenbach S, Burgstahler C, Dill T, Fischbach R, Knez A, Moshage W, Richartz BM, Ropers D, Schroder S, Silber S, Mohlenkamp S, Working group "Cardiac CTotGCS. (2010) Safety, efficacy, and indications of beta-adrenergic receptor blockade to reduce heart rate prior to coronary CT angiography. *Radiology*, 257: 614-623.

8. Pannu HK, Alvarez W, Jr., Fishman EK. (2006) Beta-blockers for cardiac CT: a primer for the radiologist. *AJR Am J Roentgenol*, 186: S341-345.
9. Maffei E, Palumbo AA, Martini C, Tedeschi C, Tarantini G, Seitun S, Ruffini L, Aldrovandi A, Weustink AC, Meijboom WB, Mollet NR, Krestin GP, de Feyter PJ, Cademartiri F. (2009) "In-house" pharmacological management for computed tomography coronary angiography: heart rate reduction, timing and safety of different drugs used during patient preparation. *Eur Radiol*, 19: 2931-2940.
10. Agatston AS, Janowitz WR, Hildner FJ, Zusmer NR, Viamonte M, Jr., Detrano R. (1990) Quantification of coronary artery calcium using ultrafast computed tomography. *J Am Coll Cardiol*, 15: 827-832.
11. Weigold WG, Abbara S, Achenbach S, Arbab-Zadeh A, Berman D, Carr JJ, Cury RC, Halliburton SS, McCollough CH, Taylor AJ, Society of Cardiovascular Computed T. (2011) Standardized medical terminology for cardiac computed tomography: a report of the Society of Cardiovascular Computed Tomography. *J Cardiovasc Comput Tomogr*, 5: 136-144.
12. Leipsic J, Abbara S, Achenbach S, Cury R, Earls JP, Mancini GJ, Nieman K, Pontone G, Raff GL. (2014) SCCT guidelines for the interpretation and reporting of coronary CT angiography: a report of the Society of Cardiovascular Computed Tomography Guidelines Committee. *J Cardiovasc Comput Tomogr*, 8: 342-358.
13. Ritchie CJ, Godwin JD, Crawford CR, Stanford W, Anno H, Kim Y. (1992) Minimum scan speeds for suppression of motion artifacts in CT. *Radiology*, 185: 37-42.
14. Hsiao EM, Rybicki FJ, Steigner M. (2010) CT coronary angiography: 256-slice and 320-detector row scanners. *Curr Cardiol Rep*, 12: 68-75.
15. Husmann L, Leschka S, Desbiolles L, Schepis T, Gaemperli O, Seifert B, Cattin P, Frauenfelder T, Flohr TG, Marincek B, Kaufmann PA, Alkadhi H. (2007) Coronary artery motion and cardiac phases: dependency on heart rate -- implications for CT image reconstruction. *Radiology*, 245: 567-576.
16. Hausleiter J, Meyer TS, Martuscelli E, Spagnolo P, Yamamoto H, Carrascosa P, Anger T, Lehmkuhl L, Alkadhi H, Martinoff S, Hadamitzky M, Hein F,

- Bischoff B, Kuse M, Schomig A, Achenbach S. (2012) Image quality and radiation exposure with prospectively ECG-triggered axial scanning for coronary CT angiography: the multicenter, multivendor, randomized PROTECTION-III study. *JACC Cardiovasc Imaging*, 5: 484-493.
17. Giesler T, Baum U, Ropers D, Ulzheimer S, Wenkel E, Mennicke M, Bautz W, Kalender WA, Daniel WG, Achenbach S. (2002) Noninvasive visualization of coronary arteries using contrast-enhanced multidetector CT: influence of heart rate on image quality and stenosis detection. *AJR Am J Roentgenol*, 179: 911-916.
 18. Schroeder S, Kopp AF, Kuettner A, Burgstahler C, Herdeg C, Heuschmid M, Baumbach A, Claussen CD, Karsch KR, Seipel L. (2002) Influence of heart rate on vessel visibility in noninvasive coronary angiography using new multislice computed tomography: experience in 94 patients. *Clin Imaging*, 26: 106-111.
 19. Raff GL, Gallagher MJ, O'Neill WW, Goldstein JA. (2005) Diagnostic accuracy of noninvasive coronary angiography using 64-slice spiral computed tomography. *J Am Coll Cardiol*, 46: 552-557.
 20. Hausleiter J, Meyer T, Hermann F, Hadamitzky M, Krebs M, Gerber TC, McCollough C, Martinoff S, Kastrati A, Schomig A, Achenbach S. (2009) Estimated radiation dose associated with cardiac CT angiography. *JAMA*, 301: 500-507.
 21. Gerber TC, Carr JJ, Arai AE, Dixon RL, Ferrari VA, Gomes AS, Heller GV, McCollough CH, McNitt-Gray MF, Mettler FA, Mieres JH, Morin RL, Yester MV. (2009) Ionizing radiation in cardiac imaging: a science advisory from the American Heart Association Committee on Cardiac Imaging of the Council on Clinical Cardiology and Committee on Cardiovascular Imaging and Intervention of the Council on Cardiovascular Radiology and Intervention. *Circulation*, 119: 1056-1065.
 22. Coles DR, Smail MA, Negus IS, Wilde P, Oberhoff M, Karsch KR, Baumbach A. (2006) Comparison of radiation doses from multislice computed tomography coronary angiography and conventional diagnostic angiography. *J Am Coll Cardiol*, 47: 1840-1845.

23. Halliburton SS, Abbara S, Chen MY, Gentry R, Mahesh M, Raff GL, Shaw LJ, Hausleiter J, Society of Cardiovascular Computed T. (2011) SCCT guidelines on radiation dose and dose-optimization strategies in cardiovascular CT. *J Cardiovasc Comput Tomogr*, 5: 198-224.
24. Earls JP, Berman EL, Urban BA, Curry CA, Lane JL, Jennings RS, McCulloch CC, Hsieh J, Londt JH. (2008) Prospectively gated transverse coronary CT angiography versus retrospectively gated helical technique: improved image quality and reduced radiation dose. *Radiology*, 246: 742-753.
25. Maruyama T, Takada M, Hasuike T, Yoshikawa A, Namimatsu E, Yoshizumi T. (2008) Radiation dose reduction and coronary assessability of prospective electrocardiogram-gated computed tomography coronary angiography: comparison with retrospective electrocardiogram-gated helical scan. *J Am Coll Cardiol*, 52: 1450-1455.
26. Shuman WP, Branch KR, May JM, Mitsumori LM, Lockhart DW, Dubinsky TJ, Warren BH, Caldwell JH. (2008) Prospective versus retrospective ECG gating for 64-detector CT of the coronary arteries: comparison of image quality and patient radiation dose. *Radiology*, 248: 431-437.
27. Flohr TG, McCollough CH, Bruder H, Petersilka M, Gruber K, Suss C, Grasruck M, Stierstorfer K, Krauss B, Raupach R, Primak AN, Kuttner A, Achenbach S, Becker C, Kopp A, Ohnesorge BM. (2006) First performance evaluation of a dual-source CT (DSCT) system. *Eur Radiol*, 16: 256-268.
28. Husmann L, Valenta I, Gaemperli O, Adda O, Treyer V, Wyss CA, Veit-Haibach P, Tatsugami F, von Schulthess GK, Kaufmann PA. (2008) Feasibility of low-dose coronary CT angiography: first experience with prospective ECG-gating. *Eur Heart J*, 29: 191-197.
29. Stolzmann P, Leschka S, Scheffel H, Krauss T, Desbiolles L, Plass A, Genoni M, Flohr TG, Wildermuth S, Marincek B, Alkadhi H. (2008) Dual-source CT in step-and-shoot mode: noninvasive coronary angiography with low radiation dose. *Radiology*, 249: 71-80.
30. Herzog C, Arning-Erb M, Zangos S, Eichler K, Hammerstingl R, Dogan S, Ackermann H, Vogl TJ. (2006) Multi-detector row CT coronary angiography:

- influence of reconstruction technique and heart rate on image quality. *Radiology*, 238: 75-86.
31. Chung CS, Karamanoglu M, Kovacs SJ. (2004) Duration of diastole and its phases as a function of heart rate during supine bicycle exercise. *Am J Physiol Heart Circ Physiol*, 287: H2003-2008.
 32. Luisada AA, MacCanon DM. (1972) The phases of the cardiac cycle. *Am Heart J*, 83: 705-711.
 33. Gharib AM, Herzka DA, Ustun AO, Desai MY, Locklin J, Pettigrew RI, Stuber M. (2007) Coronary MR angiography at 3T during diastole and systole. *J Magn Reson Imaging*, 26: 921-926.
 34. Shin T, Pohost GM, Nayak KS. (2010) Systolic 3D first-pass myocardial perfusion MRI: Comparison with diastolic imaging in healthy subjects. *Magn Reson Med*, 63: 858-864.
 35. Herzog C, Abolmaali N, Balzer JO, Baunach S, Ackermann H, Dogan S, Britten MB, Vogl TJ. (2002) Heart-rate-adapted image reconstruction in multidetector-row cardiac CT: influence of physiological and technical prerequisite on image quality. *Eur Radiol*, 12: 2670-2678.
 36. Marwan M, Hausleiter J, Abbara S, Hoffmann U, Becker C, Ovrehus K, Ropers D, Bathina R, Berman D, Anders K, Uder M, Meave A, Alexanderson E, Achenbach S. (2014) Multicenter Evaluation Of Coronary Dual-Source CT angiography in patients with intermediate Risk of Coronary Artery Stenoses (MEDIC): study design and rationale. *J Cardiovasc Comput Tomogr*, 8: 183-188.
 37. Johnson TR, Nikolaou K, Wintersperger BJ, Leber AW, von Ziegler F, Rist C, Buhmann S, Knez A, Reiser MF, Becker CR. (2006) Dual-source CT cardiac imaging: initial experience. *Eur Radiol*, 16: 1409-1415.
 38. Mollet NR, Cademartiri F, de Feyter PJ. (2005) Non-invasive multislice CT coronary imaging. *Heart*, 91: 401-407.
 39. Pannu HK, Flohr TG, Corl FM, Fishman EK. (2003) Current concepts in multi-detector row CT evaluation of the coronary arteries: principles, techniques, and anatomy. *Radiographics*, 23 Spec No: S111-125.

40. Johnson PT, Eng J, Pannu HK, Fishman EK. (2008) 64-MDCT angiography of the coronary arteries: nationwide survey of patient preparation practice. *AJR Am J Roentgenol*, 190: 743-747.
41. Wiest D. (1995) Esmolol. A review of its therapeutic efficacy and pharmacokinetic characteristics. *Clin Pharmacokinet*, 28: 190-202.
42. Wiest DB, Haney JS. (2012) Clinical pharmacokinetics and therapeutic efficacy of esmolol. *Clin Pharmacokinet*, 51: 347-356.
43. Parker JD, Parker JO. (1998) Nitrate therapy for stable angina pectoris. *N Engl J Med*, 338: 520-531.
44. Armstrong PW, Armstrong JA, Marks GS. (1979) Blood levels after sublingual nitroglycerin. *Circulation*, 59: 585-588.
45. Takx RA, Sucha D, Park J, Leiner T, Hoffmann U. (2015) Sublingual Nitroglycerin Administration in Coronary Computed Tomography Angiography: a Systematic Review. *Eur Radiol*, 25: 3536-3542.
46. Pfister M, Seiler C, Fleisch M, Gobel H, Luscher T, Meier B. (1998) Nitrate induced coronary vasodilatation: differential effects of sublingual application by capsule or spray. *Heart*, 80: 365-369.
47. Thadani U, Rodgers T. (2006) Side effects of using nitrates to treat angina. *Expert Opin Drug Saf*, 5: 667-674.
48. Williams DO, Amsterdam EA, Mason DT. (1975) Hemodynamic effects of nitroglycerin in acute myocardial infarction. *Circulation*, 51: 421-427.
49. Chun EJ, Lee W, Choi YH, Koo BK, Choi SI, Jae HJ, Kim HC, So YH, Chung JW, Park JH. (2008) Effects of nitroglycerin on the diagnostic accuracy of electrocardiogram-gated coronary computed tomography angiography. *J Comput Assist Tomogr*, 32: 86-92.
50. Decramer I, Vanhoenacker PK, Sarno G, Van Hoe L, Bladt O, Wijns W, Parizel PM. (2008) Effects of sublingual nitroglycerin on coronary lumen diameter and number of visualized septal branches on 64-MDCT angiography. *AJR Am J Roentgenol*, 190: 219-225.
51. Zhang J, Fletcher JG, Scott Harmsen W, Araoz PA, Williamson EE, Primak AN, McCollough CH. (2008) Analysis of heart rate and heart rate variation during cardiac CT examinations. *Acad Radiol*, 15: 40-48.

52. Sato K, Isobe S, Sugiura K, Mimura T, Yotsudake Y, Meno C, Kato M, Harada K, Murohara T. (2009) Optimal starting time of acquisition and feasibility of complementary administration of nitroglycerin with intravenous beta-blocker in multislice computed tomography. *J Comput Assist Tomogr*, 33: 193-198.
53. Okada M, Nakashima Y, Nomura T, Miura T, Nao T, Yoshimura M, Sano Y, Matsunaga N. (2015) Coronary vasodilation by the use of sublingual nitroglycerin using 64-slice dual-source coronary computed tomography angiography. *J Cardiol*, 65: 230-236.
54. Anderson RH. (2000) Clinical anatomy of the aortic root. *Heart*, 84: 670-673.
55. Piazza N, de Jaegere P, Schultz C, Becker AE, Serruys PW, Anderson RH. (2008) Anatomy of the aortic valvar complex and its implications for transcatheter implantation of the aortic valve. *Circ Cardiovasc Interv*, 1: 74-81.
56. Albes JM, Stock UA, Hartrumpf M. (2005) Restitution of the aortic valve: what is new, what is proven, and what is obsolete? *Ann Thorac Surg*, 80: 1540-1549.
57. Sutton JP, 3rd, Ho SY, Anderson RH. (1995) The forgotten interleaflet triangles: a review of the surgical anatomy of the aortic valve. *Ann Thorac Surg*, 59: 419-427.
58. Lang RM, Bierig M, Devereux RB, Flachskampf FA, Foster E, Pellikka PA, Picard MH, Roman MJ, Seward J, Shanewise JS, Solomon SD, Spencer KT, Sutton MS, Stewart WJ, Chamber Quantification Writing G, American Society of Echocardiography's G, Standards C, European Association of E. (2005) Recommendations for chamber quantification: a report from the American Society of Echocardiography's Guidelines and Standards Committee and the Chamber Quantification Writing Group, developed in conjunction with the European Association of Echocardiography, a branch of the European Society of Cardiology. *J Am Soc Echocardiogr*, 18: 1440-1463.
59. Anderson RH, Lal M, Ho SY. (1996) Anatomy of the aortic root with particular emphasis on options for its surgical enlargement. *J Heart Valve Dis*, 5 Suppl 3: S249-257.
60. Tops LF, Wood DA, Delgado V, Schuijff JD, Mayo JR, Pasupati S, Lamers FP, van der Wall EE, Schalij MJ, Webb JG, Bax JJ. (2008) Noninvasive evaluation

- of the aortic root with multislice computed tomography implications for transcatheter aortic valve replacement. *JACC Cardiovasc Imaging*, 1: 321-330.
61. Buellesfeld L, Stortecky S, Kalesan B, Gloekler S, Khattab AA, Nietlispach F, Delfino V, Huber C, Eberle B, Meier B, Wenaweser P, Windecker S. (2013) Aortic root dimensions among patients with severe aortic stenosis undergoing transcatheter aortic valve replacement. *JACC Cardiovasc Interv*, 6: 72-83.
 62. Nicod P, Bloor C, Godfrey M, Hollister D, Pyeritz RE, Dittrich H, Polikar R, Peterson KL. (1989) Familial aortic dissecting aneurysm. *J Am Coll Cardiol*, 13: 811-819.
 63. Bella JN, MacCluer JW, Roman MJ, Almasy L, North KE, Welty TK, Lee ET, Fabsitz RR, Howard BV, Devereux RB. (2002) Genetic influences on aortic root size in American Indians: the Strong Heart Study. *Arterioscler Thromb Vasc Biol*, 22: 1008-1011.
 64. Roman MJ, Devereux RB, Kramer-Fox R, O'Loughlin J. (1989) Two-dimensional echocardiographic aortic root dimensions in normal children and adults. *Am J Cardiol*, 64: 507-512.
 65. Kim M, Roman MJ, Cavallini MC, Schwartz JE, Pickering TG, Devereux RB. (1996) Effect of hypertension on aortic root size and prevalence of aortic regurgitation. *Hypertension*, 28: 47-52.
 66. Covella M, Milan A, Totaro S, Caotaro A-H, Cuspidi C, Re A, Rabbia F, Veglio F. (2014) Echocardiographic aortic root dilatation in hypertensive patients: a systematic review and meta-analysis. *J Hypertens*, 32: 1928-1935.
 67. Jin Y, Kuznetsova T, Bochud M, Richart T, Thijs L, Cusi D, Fagard R, Staessen JA. (2011) Heritability of left ventricular structure and function in Caucasian families. *Eur J Echocardiogr*, 12: 326-332.
 68. Tzikas A, Schultz CJ, Piazza N, Moelker A, Van Mieghem NM, Nuis RJ, van Geuns RJ, Geleijnse ML, Serruys PW, de Jaegere PP. (2011) Assessment of the aortic annulus by multislice computed tomography, contrast aortography, and trans-thoracic echocardiography in patients referred for transcatheter aortic valve implantation. *Catheter Cardiovasc Interv*, 77: 868-875.

69. Ocak I, Lacomis JM, Deible CR, Pealer K, Parag Y, Knollmann F. (2009) The aortic root: comparison of measurements from ECG-gated CT angiography with transthoracic echocardiography. *J Thorac Imaging*, 24: 223-226.
70. Christian JC, Kang KW, Norton JJ, Jr. (1974) Choice of an estimate of genetic variance from twin data. *Am J Hum Genet*, 26: 154-161.
71. Vasani RS, Larson MG, Levy D. (1995) Determinants of echocardiographic aortic root size. The Framingham Heart Study. *Circulation*, 91: 734-740.
72. Ingelsson E, Pencina MJ, Levy D, Aragam J, Mitchell GF, Benjamin EJ, Vasani RS. (2008) Aortic root diameter and longitudinal blood pressure tracking. *Hypertension*, 52: 473-477.
73. Ghoshhajra BB, Engel LC, Karolyi M, Sidhu MS, Wai B, Barreto M, Shanmugam U, Hoffmann U, Brady TJ, Kalra M, Abbara S. (2013) Cardiac computed tomography angiography with automatic tube potential selection: effects on radiation dose and image quality. *J Thorac Imaging*, 28: 40-48.
74. Lee AM, Engel LC, Shah B, Liew G, Sidhu MS, Kalra M, Abbara S, Brady TJ, Hoffmann U, Ghoshhajra BB. (2012) Coronary computed tomography angiography during arrhythmia: Radiation dose reduction with prospectively ECG-triggered axial and retrospectively ECG-gated helical 128-slice dual-source CT. *J Cardiovasc Comput Tomogr*, 6: 172-183 e172.
75. Celeng C, Vadvala H, Puchner S, Pursnani A, Sharma U, Kovacs A, Maurovich-Horvat P, Hoffmann U, Ghoshhajra B. (2016) Defining the optimal systolic phase targets using absolute delay time for reconstructions in dual-source coronary CT angiography. *Int J Cardiovasc Imaging*, 32: 91-100.
76. Taylor AJ, Cerqueira M, Hodgson JM, Mark D, Min J, O'Gara P, Rubin GD, American College of Cardiology Foundation Appropriate Use Criteria Task F, Society of Cardiovascular Computed T, American College of R, American Heart A, American Society of E, American Society of Nuclear C, North American Society for Cardiovascular I, Society for Cardiovascular A, Interventions, Society for Cardiovascular Magnetic R. (2010) ACCF/SCCT/ACR/AHA/ASE/ASNC/NASCI/SCAI/SCMR 2010 Appropriate Use Criteria for Cardiac Computed Tomography. A Report of the American College of Cardiology Foundation Appropriate Use Criteria Task Force, the

- Society of Cardiovascular Computed Tomography, the American College of Radiology, the American Heart Association, the American Society of Echocardiography, the American Society of Nuclear Cardiology, the North American Society for Cardiovascular Imaging, the Society for Cardiovascular Angiography and Interventions, and the Society for Cardiovascular Magnetic Resonance. *J Cardiovasc Comput Tomogr*, 4: 407 e401-433.
77. Maurovich-Horvat P, Karolyi M, Horvath T, Szilveszter B, Bartykowszki A, Jermendy AL, Panajotu A, Celeng C, Suhai FI, Major GP, Csobay-Novak C, Huttl K, Merkely B. (2015) Esmolol is noninferior to metoprolol in achieving a target heart rate of 65 beats/min in patients referred to coronary CT angiography: a randomized controlled clinical trial. *J Cardiovasc Comput Tomogr*, 9: 139-145.
 78. Schroeder S, Achenbach S, Bengel F, Burgstahler C, Cademartiri F, de Feyter P, George R, Kaufmann P, Kopp AF, Knuuti J, Ropers D, Schuijf J, Tops LF, Bax JJ, Working Group Nuclear C, Cardiac CT, European Society of C, European Council of Nuclear C. (2008) Cardiac computed tomography: indications, applications, limitations, and training requirements: report of a Writing Group deployed by the Working Group Nuclear Cardiology and Cardiac CT of the European Society of Cardiology and the European Council of Nuclear Cardiology. *Eur Heart J*, 29: 531-556.
 79. Maurovich-Horvat P, Tarnoki DL, Tarnoki AD, Horvath T, Jermendy AL, Kolossvary M, Szilveszter B, Voros V, Kovacs A, Molnar AA, Littvay L, Lamb HJ, Voros S, Jermendy G, Merkely B. (2015) Rationale, Design, and Methodological Aspects of the BUDAPEST-GLOBAL Study (Burden of Atherosclerotic Plaques Study in Twins-Genetic Loci and the Burden of Atherosclerotic Lesions). *Clin Cardiol*, 38: 699-707.
 80. Littvay L, Metneki J, Tarnoki AD, Tarnoki DL. (2013) The Hungarian Twin Registry. *Twin Res Hum Genet*, 16: 185-189.
 81. Celeng C, Kolossvary M, Kovacs A, Molnar AA, Szilveszter B, Horvath T, Karolyi M, Jermendy AL, Tarnoki AD, Tarnoki DL, Karady J, Voros S, Jermendy G, Merkely B, Maurovich-Horvat P. (2016) Aortic root dimensions

- are predominantly determined by genetic factors: a classical twin study. *Eur Radiol*, In press.
82. Roberts WT, Wright AR, Timmis JB, Timmis AD. (2009) Safety and efficacy of a rate control protocol for cardiac CT. *Br J Radiol*, 82: 267-271.
 83. R Core Team (2015), R: A language and environment for statistical computing. R Foundation for Statistical Computing, Vienna, Austria.
 84. Kottner J, Audige L, Brorson S, Donner A, Gajewski BJ, Hrobjartsson A, Roberts C, Shoukri M, Streiner DL. (2011) Guidelines for Reporting Reliability and Agreement Studies (GRRAS) were proposed. *J Clin Epidemiol*, 64: 96-106.
 85. Neale MC, Hunter MD, Pritikin JN, Zahery M, Brick TR, Kirkpatrick RM, Estabrook R, Bates TC, Maes HH, Boker SM. (2015) OpenMx 2.0: Extended Structural Equation and Statistical Modeling. *Psychometrika*.
 86. Neale MC, Cardon LR. *Methodology for Genetic Studies of Twins and Families*. 1992: Springer, Netherlands, 87-108.
 87. Thomas Lumley using Fortran code by Alan Miller (2009), leaps: regression subset selection. R package version 2.9.
 88. Wang Y, Vidan E, Bergman GW. (1999) Cardiac motion of coronary arteries: variability in the rest period and implications for coronary MR angiography. *Radiology*, 213: 751-758.
 89. Boudoulas H, Geleris P, Lewis RP, Rittgers SE. (1981) Linear relationship between electrical systole, mechanical systole, and heart rate. *Chest*, 80: 613-617.
 90. Adler G, Meille L, Rohnean A, Sigal-Cinqualbre A, Capderou A, Paul JF. (2010) Robustness of end-systolic reconstructions in coronary dual-source CT angiography for high heart rate patients. *Eur Radiol*, 20: 1118-1123.
 91. Kim HY, Lee JW, Hong YJ, Lee HJ, Hur J, Nam JE, Choi BW, Kim YJ. (2012) Dual-source coronary CT angiography in patients with high heart rates using a prospectively ECG-triggered axial mode at end-systole. *Int J Cardiovasc Imaging*, 28 Suppl 2: 101-107.
 92. Paul JF, Amato A, Rohnean A. (2013) Low-dose coronary-CT angiography using step and shoot at any heart rate: comparison of image quality at systole for

- high heart rate and diastole for low heart rate with a 128-slice dual-source machine. *Int J Cardiovasc Imaging*, 29: 651-657.
93. Fabian J, Epstein EJ, Coulshed N. (1972) Duration of phases of left ventricular systole using indirect methods. I. Normal subjects. *Br Heart J*, 34: 874-881.
 94. Bloomfield GS, Gillam LD, Hahn RT, Kapadia S, Leipsic J, Lerakis S, Tuzcu M, Douglas PS. (2012) A practical guide to multimodality imaging of transcatheter aortic valve replacement. *JACC Cardiovasc Imaging*, 5: 441-455.
 95. Wang Y, Qin L, Shi X, Zeng Y, Jing H, Schoepf UJ, Jin Z. (2012) Adenosine-stress dynamic myocardial perfusion imaging with second-generation dual-source CT: comparison with conventional catheter coronary angiography and SPECT nuclear myocardial perfusion imaging. *AJR Am J Roentgenol*, 198: 521-529.
 96. Taillefer R, Ahlberg AW, Masood Y, White CM, Lamargese I, Mather JF, McGill CC, Heller GV. (2003) Acute beta-blockade reduces the extent and severity of myocardial perfusion defects with dipyridamole Tc-99m sestamibi SPECT imaging. *J Am Coll Cardiol*, 42: 1475-1483.
 97. Degertekin M, Gemici G, Kaya Z, Bayrak F, Guneyisu T, Sevinc D, Mutlu B, Aytaclar S. (2008) Safety and efficacy of patient preparation with intravenous esmolol before 64-slice computed tomography coronary angiography. *Coron Artery Dis*, 19: 33-36.
 98. Kassamali RH, Kim DH, Patel H, Raichura N, Hoey ET, Hodson J, Hussain S. (2014) Safety of an i.v. beta-adrenergic blockade protocol for heart rate optimization before coronary CT angiography. *AJR Am J Roentgenol*, 203: 759-762.
 99. Reynolds RD, Gorczynski RJ, Quon CY. (1986) Pharmacology and pharmacokinetics of esmolol. *J Clin Pharmacol*, 26 Suppl A: A3-A14.
 100. Oxorn D, Knox JW, Hill J. (1990) Bolus doses of esmolol for the prevention of perioperative hypertension and tachycardia. *Can J Anaesth*, 37: 206-209.
 101. Parnass SM, Rothenberg DM, Kerchberger JP, Ivankovich AD. (1990) A single bolus dose of esmolol in the prevention of intubation-induced tachycardia and hypertension in an ambulatory surgery unit. *J Clin Anesth*, 2: 232-237.

102. Sheppard D, DiStefano S, Byrd RC, Eschenbacher WL, Bell V, Steck J, Laddu A. (1986) Effects of esmolol on airway function in patients with asthma. *J Clin Pharmacol*, 26: 169-174.
103. Messika-Zeitoun D, Serfaty JM, Brochet E, Ducrocq G, Lepage L, Detaint D, Hyafil F, Himbert D, Pasi N, Laissy JP, Iung B, Vahanian A. (2010) Multimodal assessment of the aortic annulus diameter: implications for transcatheter aortic valve implantation. *J Am Coll Cardiol*, 55: 186-194.
104. Pannu H, Fadulu VT, Chang J, Lafont A, Hasham SN, Sparks E, Giampietro PF, Zaleski C, Estrera AL, Safi HJ, Shete S, Willing MC, Raman CS, Milewicz DM. (2005) Mutations in transforming growth factor-beta receptor type II cause familial thoracic aortic aneurysms and dissections. *Circulation*, 112: 513-520.
105. Loeys BL, Schwarze U, Holm T, Callewaert BL, Thomas GH, Pannu H, De Backer JF, Oswald GL, Symoens S, Manouvrier S, Roberts AE, Faravelli F, Greco MA, Pyeritz RE, Milewicz DM, Coucke PJ, Cameron DE, Braverman AC, Byers PH, De Paepe AM, Dietz HC. (2006) Aneurysm syndromes caused by mutations in the TGF-beta receptor. *N Engl J Med*, 355: 788-798.
106. Schlatmann TJ, Becker AE. (1977) Pathogenesis of dissecting aneurysm of aorta. Comparative histopathologic study of significance of medial changes. *Am J Cardiol*, 39: 21-26.
107. Bertoli-Avella AM, Gillis E, Morisaki H, Verhagen JM, de Graaf BM, van de Beek G, Gallo E, Kruithof BP, Venselaar H, Myers LA, Laga S, Doyle AJ, Oswald G, van Cappellen GW, Yamanaka I, van der Helm RM, Beverloo B, de Klein A, Pardo L, Lammens M, Evers C, Devriendt K, Dumoulein M, Timmermans J, Bruggenwirth HT, Verheijen F, Rodrigus I, Baynam G, Kempers M, Saenen J, Van Craenenbroeck EM, Minatoya K, Matsukawa R, Tsukube T, Kubo N, Hofstra R, Goumans MJ, Bekkers JA, Roos-Hesselink JW, van de Laar IM, Dietz HC, Van Laer L, Morisaki T, Wessels MW, Loeys BL. (2015) Mutations in a TGF-beta ligand, TGFB3, cause syndromic aortic aneurysms and dissections. *J Am Coll Cardiol*, 65: 1324-1336.
108. Jimenez-Juan L, Nguyen ET, Wintersperger BJ, Moshonov H, Crean AM, Deva DP, Paul NS, Torres FS. (2013) Failed heart rate control with oral metoprolol prior to coronary CT angiography: effect of additional intravenous metoprolol

- on heart rate, image quality and radiation dose. *Int J Cardiovasc Imaging*, 29: 199-206.
109. Martinez MW, Kirsch J, Williamson EE, Syed IS, Feng D, Ommen S, Packer DL, Brady PA. (2009) Utility of nongated multidetector computed tomography for detection of left atrial thrombus in patients undergoing catheter ablation of atrial fibrillation. *JACC Cardiovasc Imaging*, 2: 69-76.
 110. Krahn AD, Manfreda J, Tate RB, Mathewson FA, Cuddy TE. (1995) The natural history of atrial fibrillation: incidence, risk factors, and prognosis in the Manitoba Follow-Up Study. *Am J Med*, 98: 476-484.
 111. Hohnloser SH, Crijns HJ, van Eickels M, Gaudin C, Page RL, Torp-Pedersen C, Connolly SJ, Investigators A. (2009) Effect of dronedarone on cardiovascular events in atrial fibrillation. *N Engl J Med*, 360: 668-678.
 112. Leipsic J, Gurvitch R, Labounty TM, Min JK, Wood D, Johnson M, Ajlan AM, Wijesinghe N, Webb JG. (2011) Multidetector computed tomography in transcatheter aortic valve implantation. *JACC Cardiovasc Imaging*, 4: 416-429.
 113. Hamdan A, Guetta V, Konen E, Goitein O, Segev A, Raanani E, Spiegelstein D, Hay I, Di Segni E, Eldar M, Schwammenthal E. (2012) Deformation dynamics and mechanical properties of the aortic annulus by 4-dimensional computed tomography: insights into the functional anatomy of the aortic valve complex and implications for transcatheter aortic valve therapy. *J Am Coll Cardiol*, 59: 119-127.
 114. Watanabe Y, Morice MC, Bouvier E, Leong T, Hayashida K, Lefevre T, Hovasse T, Romano M, Chevalier B, Donzeau-Gouge P, Farge A, Cormier B, Garot P. (2013) Automated 3-dimensional aortic annular assessment by multidetector computed tomography in transcatheter aortic valve implantation. *JACC Cardiovasc Interv*, 6: 955-964.
 115. de Roos A. (2010) Myocardial perfusion imaging with multidetector CT: beyond lumenography. *Radiology*, 254: 321-323.
 116. Feuchtner G, Goetti R, Plass A, Wieser M, Scheffel H, Wyss C, Stolzmann P, Donati O, Schnabl J, Falk V, Alkadhi H, Leschka S, Cury RC. (2011) Adenosine stress high-pitch 128-slice dual-source myocardial computed tomography perfusion for imaging of reversible myocardial ischemia:

- comparison with magnetic resonance imaging. *Circ Cardiovasc Imaging*, 4: 540-549.
117. De Cecco CN, Harris BS, Schoepf UJ, Silverman JR, McWhite CB, Krazinski AW, Bayer RR, Meinel FG. (2014) Incremental value of pharmacological stress cardiac dual-energy CT over coronary CT angiography alone for the assessment of coronary artery disease in a high-risk population. *AJR Am J Roentgenol*, 203: W70-77.
118. O'Neill B, Wang DD, Pantelic M, Song T, Guerrero M, Greenbaum A, O'Neill WW. (2015) Transcatheter caval valve implantation using multimodality imaging: roles of TEE, CT, and 3D printing. *JACC Cardiovasc Imaging*, 8: 221-225.

10. BIBLIOGRAPHY OF THE CANDIDATE'S PUBLICATIONS

10.1 Publications closely related to the present thesis

1. **Celeng C**, Vadvala H, Puchner S, Pursnani A, Sharma U, Kovacs A, Maurovich-Horvat P, Hoffmann U, Ghoshhajra B. (2016) Defining the optimal systolic phase targets using absolute delay time for reconstructions in dual-source coronary CT angiography. *Int J Cardiovasc Imaging*, 32: 91-100.
2. **Celeng C**, Kolossvary M, Kovacs A, Molnar AA, Szilveszter B, Horvath T, Karolyi M, Jermendy AL, Tarnoki AD, Tarnoki DL, Karady J, Voros S, Jermendy G, Merkely B, Maurovich-Horvat P. (2016) Aortic root dimensions are predominantly determined by genetic factors: a classical twin study. *Eur Radiol*. In press
3. Maurovich-Horvat P, Karolyi M, Horvath T, Szilveszter B, Bartykowszki A, Jermendy AL, Panajotu A, **Celeng C**, Suhai FI, Major GP, Csobay-Novak C, Huttl K, Merkely B. (2015) Esmolol is noninferior to metoprolol in achieving a target heart rate of 65 beats/min in patients referred to coronary CT angiography: a randomized controlled clinical trial. *J Cardiovasc Comput Tomogr*, 9: 139-145.

10.2 Publications not related to the present thesis

1. **Celeng C**, Takx RA, Ferencik M, Maurovich-Horvat P. (2016) Non-invasive and invasive imaging of vulnerable coronary plaque. *Trends Cardiovasc Med*, 26: 538-547.
2. **Celeng C**, Maurovich-Horvat P, Ghoshhajra BB, Merkely B, Leiner T, Takx RA. (2016) Prognostic Value of Coronary Computed Tomography Angiography in Patients With Diabetes: A Meta-analysis. *Diabetes Care*, 39: 1274-1280.
3. Kovacs A, Molnar AA, **Celeng C**, Toth A, Vago H, Apor A, Tarnoki AD, Tarnoki DL, Kosa J, Lakatos P, Voros S, Jermendy G, Merkely B, Maurovich-Horvat P. (2016) Hypertrophic Cardiomyopathy in a Monozygotic Twin Pair: Similarly Different. *Circ Cardiovasc Imaging*, 9: 1-7.

4. Pursnani A, **Celeng C**, Schlett CL, Mayrhofer T, Zakrotsky P, Lee H, Ferencik M, Fleg JL, Bamberg F, Wiviott SD, Truong QA, Udelson JE, Nagurney JT, Hoffmann U. (2016) Use of Coronary Computed Tomographic Angiography Findings to Modify Statin and Aspirin Prescription in Patients With Acute Chest Pain. *Am J Cardiol*, 117: 319-324.
5. Szilveszter B, **Celeng C**, Maurovich-Horvat P. (2016) Plaque assessment by coronary CT. *Int J Cardiovasc Imaging*, 32: 161-172.
6. Szilveszter B, Elzomor H, Karolyi M, Kolossvary M, Raaijmakers R, Benke K, **Celeng C**, Bartykowszki A, Bagyura Z, Lux A, Merkely B, Maurovich-Horvat P. (2016) The effect of iterative model reconstruction on coronary artery calcium quantification. *Int J Cardiovasc Imaging*, 32: 153-160.
7. **Celeng C**, Szekely L, Toth A, Denes M, Csobay-Novak C, Bartykowszki A, Karolyi M, Vago H, Szoke S, Coelho Filho OR, Andreka P, Merkely B, Maurovich-Horvat P. (2015) Multimodality Imaging of Giant Right Coronary Aneurysm and Postsurgical Coronary Artery Inflammation. *Circulation*, 132: e1-5.
8. Pursnani A, Schlett CL, Mayrhofer T, **Celeng C**, Zakrotsky P, Bamberg F, Nagurney JT, Truong QA, Hoffmann U. (2015) Potential for coronary CT angiography to tailor medical therapy beyond preventive guideline-based recommendations: insights from the ROMICAT I trial. *J Cardiovasc Comput Tomogr*, 9: 193-201.
9. Bartykowszki A, **Celeng C**, Karolyi M, Maurovich-Horvat P. (2014) High Risk Features on Coronary CT Angiography. *Curr Cardiovasc Imaging Rep*, 7: 9279.
10. Ghoshhajra BB, Lee AM, Engel LC, **Celeng C**, Kalra MK, Brady TJ, Hoffmann U, Westra SJ, Abbara S. (2014) Radiation dose reduction in pediatric cardiac computed tomography: experience from a tertiary medical center. *Pediatr Cardiol*, 35: 171-179.

11. Kovacs A, Tapolyai M, **Celeng C**, Gara E, Faludi M, Berta K, Apor A, Nagy A, Tisler A, Merkely B. (2014) Impact of hemodialysis, left ventricular mass and FGF-23 on myocardial mechanics in end-stage renal disease: a three-dimensional speckle tracking study. *Int J Cardiovasc Imaging*, 30: 1331-1337.
12. Schlett CL, Ferencik M, **Celeng C**, Maurovich-Horvat P, Scheffel H, Stolzmann P, Do S, Kauczor HU, Alkadhi H, Bamberg F, Hoffmann U. (2013) How to assess non-calcified plaque in CT angiography: delineation methods affect diagnostic accuracy of low-attenuation plaque by CT for lipid-core plaque in histology. *Eur Heart J Cardiovasc Imaging*, 14: 1099-1105.

Articles in Hungarian

1. **Celeng C**, Maurovich-Horvat P, Merkely B. (2015) Akut koronária szindróma prevenciója és kezelése. *Metabolizmus*, 13: 49-52.

ACKNOWLEDGEMENTS

During my PhD I worked together with many inspiring people and it has been a privilege to work with all of you. I would like to take this opportunity to thank all of you who stood by me in this endeavor. I want to mention several of you specifically:

Pál Maurovich-Horvat, who was my mentor during the past three years. Pál, thank you, that you trusted in me before you really got to know me, and making me a member of your team. Your enthusiasm and precision in research always inspired me throughout my doctoral work. I will never forget our nice conversations and fun times spent at the CIRG office.

Furthermore I would like to gratefully thank to Professor Béla Merkely for his constant support during my doctoral years. Dear Professor, thank you for allowing me to participate on international congresses and for all the help you provided during our FFR study. It was a great honor to sing on the Christmas parties, even bigger to be the part of your wedding.

I would like to express my thanks to Brian Ghoshhajra, who involved me into his group in Boston and supervised my first publication. Brian, thank you also for the honest conversations, letting me to go for a “second round” to Boston and that I could use your comfy office.

I am grateful to Attila Kovács, who was not just my classmate and later colleague but also my friend. Attila your endurance and confidence in research never stopped amazing me. I always liked the nice discussion we had “about the life in general”. I know you will accomplish great things. I would like to thank to Mihály Károlyi, for being my friend and colleague during the past three years. Misi, I really enjoyed our cheerful “road-trippins”. I am also grateful to Eszter Végh, whose kindness and understanding made easier the grey weekdays.

I would like to thank to all my international colleagues at the Cardiac MR PET CT Program, especially to Professor Udo Hoffmann, Dr. Christopher L. Schlett, Dr. Amit Pursnani and Dr. Umesh Sharma for their support and contribution to my research in Boston. It was a pleasure to work in this inspiring environment.

I am grateful to my former colleagues at Heart and Vascular Center. Thank you all for the continuing support and fun moments. I hope to see many of you again later in life.

I would like to thank to my fiancé Richard for his unconditional love and support he gives. Dear Richard, it is a great pleasure to be the part of your life. Thanks that you introduced me the world of meta-analyses and reviewing. I really enjoy the tour we started together.

Last, but not least I would like to thank to my beloved parents, my sister and the rest of my family for all their support and contribution.